AGU PUBLICATIONS

JGR

Journal of Geophysical Research: Solid Earth

RESEARCH ARTICLE
10.1002/2017JB014474

Key Points:
- We image 2-D anisotropic electric resistivity structure beneath the Rocky Mountains and Great Plains to depths of 150 km
- High electrical conductivity in the lower crust beneath the Rocky Mountains is attributed to partial melt and crustal fluids
- Eastward deepening mantle conductivity beneath the Great Plains is interpreted as a hydration front

Supporting Information:
- Supporting Information S1

Correspondence to:
D. W. Feucht,
daniel.feucht@colorado.edu

Citation:
Feucht, D. W., Sheehan, A. F., & Bedrosian, P. A. (2017). Magnetotelluric imaging of lower crustal melt and lithospheric hydration in the Rocky Mountain Front transition zone, Colorado, USA. *Journal of Geophysical Research: Solid Earth*, *122*, 9489–9510. https://doi.org/10.1002/2017JB014474

Received 24 MAY 2017
Accepted 2 NOV 2017
Accepted article online 6 NOV 2017
Published online 4 DEC 2017

Magnetotelluric Imaging of Lower Crustal Melt and Lithospheric Hydration in the Rocky Mountain Front Transition Zone, Colorado, USA

D. W. Feucht[1,2], A. F. Sheehan[1,2], and P. A. Bedrosian[3]

[1]Department of Geological Sciences, University of Colorado Boulder, Boulder, CO, USA, [2]Cooperative Institute for Research in Environmental Sciences, University of Colorado Boulder, Boulder, CO, USA, [3]Crustal Geophysics and Geochemistry Science Center, U.S. Geological Survey, Denver, CO, USA

Abstract We present an electrical resistivity model of the crust and upper mantle from two-dimensional (2-D) anisotropic inversion of magnetotelluric data collected along a 450 km transect of the Rio Grande rift, southern Rocky Mountains, and High Plains in Colorado, USA. Our model provides a window into the modern-day lithosphere beneath the Rocky Mountain Front to depths in excess of 150 km. Two key features of the 2-D resistivity model are (1) a broad zone (~200 km wide) of enhanced electrical conductivity (<20 Ωm) in the midcrust to lower crust that is centered beneath the highest elevations of the southern Rocky Mountains and (2) hydrated lithospheric mantle beneath the Great Plains with water content in excess of 100 ppm. We interpret the high conductivity region of the lower crust as a zone of partially molten basalt and associated deep-crustal fluids that is the result of recent (less than 10 Ma) tectonic activity in the region. The recent supply of volatiles and/or heat to the base of the crust in the late Cenozoic implies that modern-day tectonic activity in the western United States extends to at least the western margin of the Great Plains. The transition from conductive to resistive upper mantle is caused by a gradient in lithospheric modification, likely including hydration of nominally anhydrous minerals, with maximum hydration occurring beneath the Rocky Mountain Front. This lithospheric "hydration front" has implications for the tectonic evolution of the continental interior and the mechanisms by which water infiltrates the lithosphere.

1. Introduction

1.1. Geologic and Tectonic Background

The Rocky Mountain Front (RMF) is a north-south trending physiographic boundary in the west central United States that separates the Great Plains to the east from the Rocky Mountains and Basin and Range to the west (Fenneman, 1946). The Great Plains are characterized by a low-relief landscape, broad flat sedimentary packages, and anomalously high topography (>1,600 m) over a broad region east of the Rocky Mountain Front (Eaton, 1987). This topography slopes gently down to the east for nearly 900 km, finally reaching elevations <300 m at the Missouri River on the eastern border of Kansas. The absence of major faulting, structural dismemberment, and volcanism suggest that the high western plains immediately adjacent to the RMF have been largely undeformed since the Proterozoic assembly of the North American continent. Exceptions to this include (1) tilting, subsidence, and rebound in response to Farallon slab subduction, sedimentation, and subsequent slab removal (Dickinson et al., 1988; Mitrovica et al., 1989) and (2) anorogenic uplift related to lithospheric modification and dedensification caused by hydration of the lithosphere during Farallon slab subduction (Humphreys et al., 2003; Jones et al., 2015).

In contrast, the mountains to the west of the RMF are characterized by high relief and topography with the southern Rocky Mountains in Colorado representing the most significant collection of high peaks on the North American plate (Eaton, 2008). The modern landscape of the southern Rocky Mountains is the result of a protracted tectonic history extending at least as far back in time as the formation of the Ancestral Rocky Mountains in the Pennsylvanian (Mallory, 1958). Since just the Late Cretaceous, the region has been subjected to basement-cored thrust faulting associated with the Laramide orogeny (DeCelles, 2004), high-volume silicic volcanism in the Paleogene (Lipman, 1992), widespread landscape beveling during the Eocene (Epis & Chapin, 1975), and at least two distinct episodes of continental rifting along the Rio Grande

rift from the Oligocene to the modern day (Chapin & Cather, 1994; Landman & Flowers, 2013). Quaternary fault scarps (Tweto, 1979), geodetic observations (Berglund et al., 2012), seismicity (Nakai et al., 2017), and recent volcanism (Leat et al., 1989) suggest that the southern Rocky Mountains are tectonically active in the present day.

1.2. Previous Geophysical Results

Geophysical studies on both regional and continental scales suggest that the physiographic contrast observed across the Rocky Mountain Front is at least coincident with, if not indicative of, a more profound lithospheric discontinuity at depth (Pakiser & Zietz, 1965). Investigations into seismic velocity of the crust and upper mantle and seismic attenuation suggest that the Rocky Mountain Front delineates the transition between younger, actively deforming lithosphere of western North America and older, more stable Proterozoic lithosphere to the east (Boyd & Sheehan, 2005; Phillips et al., 2014; Schmandt & Lin, 2014; Schmandt et al., 2015).

Teleseismic shear wave traveltime residuals recorded by the Rocky Mountain Front Program for Array Seismic Studies of the Continental Lithosphere experiment show a distinct increase in residual delay times from east to west across the Rocky Mountain Front (Lee & Grand, 1996). Subsequent tomographic inversions of those delay times reveal a low-velocity mantle (shear wave velocity anomalies as low as −4.5% relative to preliminary reference Earth model 1981 at depths of 50–100 km) beneath the southern Rocky Mountains in central Colorado (Lee & Grand, 1996). Li et al. (2002) inverted Rayleigh-wave phase velocities from the same experiment to show that there is also a crustal low-velocity zone (shear wave velocity anomaly as low as −4% relative to a modified version of AK135) beneath the highest topography in Colorado. Recent analyses of seismic data from the EarthScope USArray and codeployed regional seismic networks (e.g., CREST (Hansen et al., 2013)) have produced a multitude of seismic-velocity models of the western United States and Rocky Mountain Front (e.g., Hansen et al., 2013; Porritt et al., 2014; Schmandt & Humphreys, 2010; Schmandt & Lin, 2014; Shen et al., 2013). A broad low-velocity zone in the upper mantle beneath Colorado west of the RMF is a common feature of each of these models. Possible explanations for the anomaly include both thermal and compositional variations in the upper mantle, including both thinned and/or chemically modified lithosphere. Low-velocity anomalies in the lower crust are typically attributed to compositional variations, specifically an abundance of low-density felsic material in the crust west of the Rocky Mountain Front (Decker et al., 1988; Li et al., 2002; Schmandt et al., 2015).

The magnetotelluric (MT) method is particularly well suited for differentiating thermal and compositional origins of geophysical anomalies within the lithosphere (e.g., Li et al., 2003; Wannamaker et al., 2008; Yang, 2011), where resolution is comparable to seismic tomography (e.g., Meqbel et al., 2014). In this paper we present results from a magnetotelluric survey in central Colorado that straddles the Rocky Mountain Front. We employ a 2-D anisotropic inverse modeling approach to determine electrical resistivity structure beneath our profile. We image (1) a zone of high conductivity in the lower crust beneath the southern Rocky Mountains and (2) distinct compositional modification of the lithospheric mantle beneath the western edge of the Great Plains. We examine the possible compositional and thermal origins of these anomalies before commenting on the tectonic implications of our preferred interpretation.

2. Methods and Data

2.1. Magnetotellurics

Magnetotelluric data are collected by measuring spatial and temporal variations in the naturally occurring electric (E) and magnetic (H) fields at the surface of the Earth. The magnetotelluric impedance tensor (Z) is a second-rank complex tensor that in the frequency domain relates horizontal magnetic fields to horizontal electric fields by

$$\begin{bmatrix} E_X \\ E_Y \end{bmatrix} = \begin{bmatrix} Z_{XX} & Z_{XY} \\ Z_{YX} & Z_{YY} \end{bmatrix} \cdot \begin{bmatrix} H_X \\ H_Y \end{bmatrix} \tag{1}$$

The four components of the complex, frequency-dependent impedance tensor can be represented as scaled amplitude (apparent resistivity, ρ_a, units of Ωm) and phase. The magnetic field transfer function

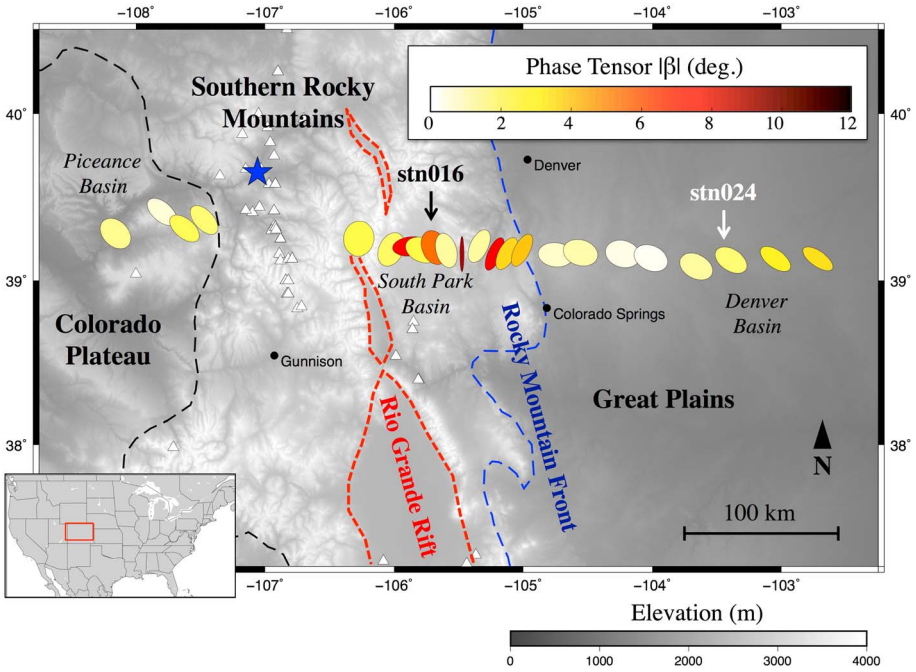

Figure 1. Map of magnetotelluric stations in central Colorado. Station locations represented by normalized magnetotelluric phase tensor ellipses at period of 1,000 s (sensitive to structure from the midcrust to upper mantle depending on resistivity structure). Phase tensor ellipse fill color is scaled by $|\beta|$, with larger values indicating 3-D structure. In the presence of 2-D electrical resistivity structure, the major axes of phase tensor ellipses will align parallel (perpendicular) to regional geoelectric strike for data collected on the resistive (conductive) side of a geoelectrical contact. Note the 90° rotation of the phase tensor ellipses across the Rocky Mountain Front (blue dashed line) that separates resistive basement-cored uplifts to the east from conductive sedimentary units of the Denver Basin to the west. The red dashed lines are approximate outlines of axial basins of the Rio Grande rift. The black and blue dashed lines are physiographic province boundaries (Fenneman, 1946). The blue star is the location of a Quaternary basalt flow near Dotsero, CO (see section 4.2). The white triangles are young volcanics (<10 Ma) from the NAVDAT database (Walker et al., 2006). Location of MT data shown in Figure 2 indicated by arrows and station labels.

(T), or tipper, is a complex unitless vector quantity that relates the horizontal magnetic field to the vertical magnetic field by

$$H_Z = [T_X \;\; T_Y] \cdot \begin{bmatrix} H_X \\ H_Y \end{bmatrix} \tag{2}$$

These transfer functions vary both spatially according to the electrical resistivity structure of the subsurface and with frequency as a function of changes in subsurface resistivity with depth. A magnetotelluric sounding consists of estimates of impedance and tipper as a function of period, obtained via spectral analysis of electromagnetic field time series. The depth of investigation of each sounding depends on both the period (the inverse of frequency) and the local electrical resistivity structure, with longer periods and a more resistive subsurface allowing for a greater depth of investigation.

The magnetotelluric method is in particular sensitive to electrical resistivity, or its reciprocal conductivity, which is dependent upon mineralogy, fluid content, partial melting, and chemical alteration of the subsurface. Sources of high conductivity in sedimentary basins and within the brittle upper crust include clay minerals, fault gouge, and groundwater. The primary controls on electrical conductivity in the lower crust are the abundance and interconnectedness of aqueous fluid, small volumes of partial melt, and grain boundary mineralization. Electrical conductivity in the upper mantle is primarily controlled by the concentration of water in nominally anhydrous minerals (Dai & Karato, 2009; Poe et al., 2010), the presence of partial melt, and to a lesser extent the bulk temperature of the rock (Constable et al., 1992).

2.2. Data

Twenty-three magnetotelluric soundings were collected in central Colorado along a 450 km profile located at 39.2°N latitude (Figure 1). Details on the data acquisition parameters can be found in the supporting

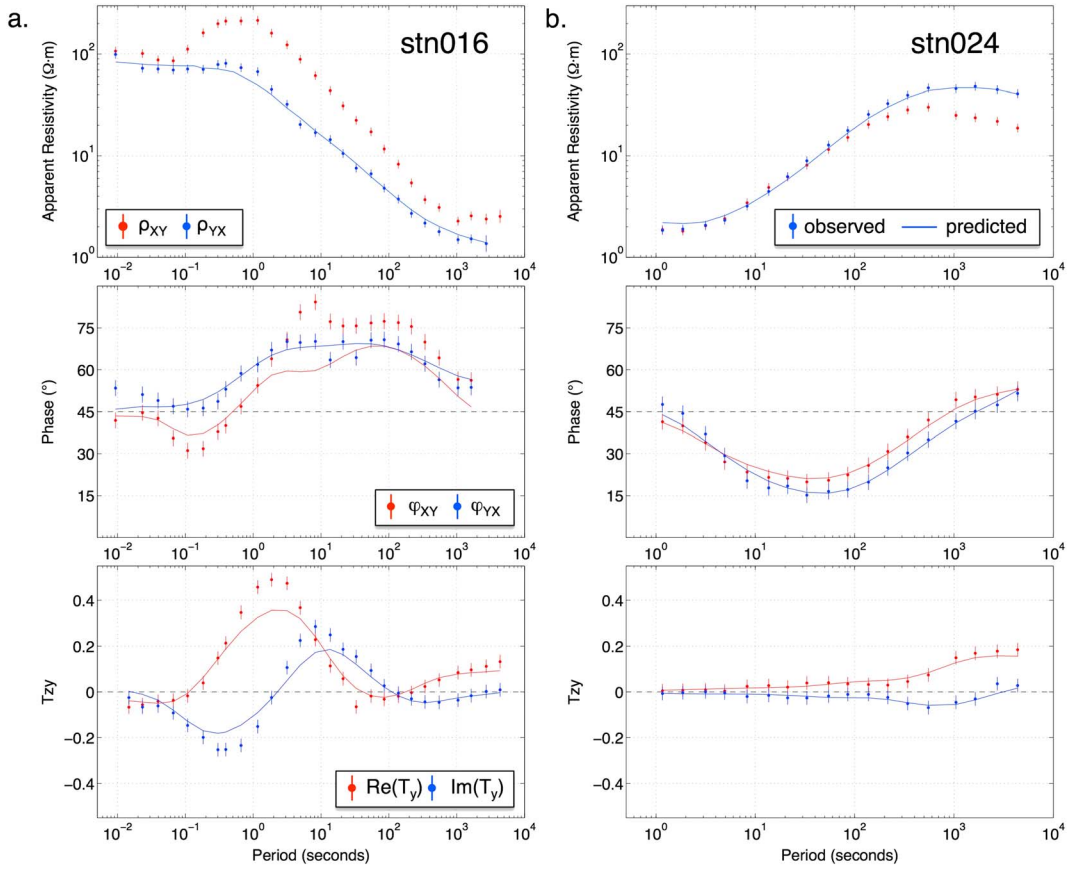

Figure 2. MT apparent resistivity, phase, and tipper (T_Y) (data points with 1 sigma uncertainty) and 2-D anisotropic model fits (solid lines) for stations (a) 016 in the mountains and (b) 024 in the plains. TE mode apparent resistivity (ρ_{XY}) omitted from the inversion inputs to reduce influence of 3-D electrical resistivity structure.

information. Time series processing and transfer function estimation were performed using the approach of Egbert (1997) for multistation arrays with remote referencing (Gamble et al., 1979). Some stations required additional preprocessing prior to transfer function estimation due to operator error, data logger malfunction, and/or station disturbance during recording. Preprocessing steps included trimming of data contaminated by cultural noise, scaling, and correction of layout errors (e.g., electric and magnetic channel flips). Figure 2 shows representative transfer function curves for two stations: stn016 located in the mountains and stn024 in the plains.

The magnetotelluric phase tensor (Caldwell et al., 2004), a mathematical transformation of the impedance tensor, is used to examine the dimensionality of MT data. Interpretation of the phase tensor is performed by examining maps of normalized phase tensor ellipses, the major and minor axes of which are proportional to the rotationally invariant maximum and minimum principal values of the represented phase tensor. Circular phase tensors reflect a one-dimensional impedance (layer-cake subsurface resistivity structure) while noncircular ellipses indicate higher-order electrical resistivity structure (e.g., lateral variations in resistivity). In the two-dimensional (2-D) case, the major axis of the ellipse will align either perpendicular or parallel to the predominant geoelectric strike for data collected on the conductive or resistive side, respectively, of a geoelectrical contact.

Figure 1 shows normalized phase tensor ellipses for all 23 MT stations at a period of 1,000 s. Note the major-axis orientation of the phase tensor ellipses changes from generally north-south to east-west moving west to east across the Rocky Mountain Front, indicating a major geoelectric contact coincident with the Rocky Mountains-Great Plains physiographic boundary. The scalar value β, another rotationally invariant phase tensor parameter, is an indicator of three-dimensional (3-D) geoelectric structure. Typically, $|\beta| > 3°$ is

considered an indication of 3-D structure (Booker, 2014). The majority of the ellipses in Figure 1 exhibit low values of β (see fill color) with either major or minor axes trending subparallel to the profile, indicating that two-dimensional inversion of the measured data is justified. We note that high β values are observed for several stations in the mountains (106°W–105°W) at a period of 1,000 s. Given the high resistivity of the plutonic and metamorphic rocks of the Rocky Mountain Front Range that underlie these particular stations, the phase tensors at the displayed period may have sensitivity to mid to lower crustal structure, indicating that the geoelectric structure is complex at depth. Quasi-3-D electrical resistivity structure is also observed in the distribution of induction vector orientations (see Figure S1 in the supporting information). The ability of the 2-D anisotropic inversion to fit these pseudo 3-D data is shown in Figure 2a for stn016. Full pseudo-sections of observed data and anisotropic model fits are provided in the supporting information.

2.3. 2-D Inversion

We invert for two-dimensional isotropic and anisotropic electrical resistivity structure along our profile using the finite element inversion algorithm MARE2DEM (Key, 2016). The MARE2DEM algorithm utilizes an Occam's inversion approach (Constable et al., 1987), which seeks to iteratively determine the smoothest possible electrical resistivity structure that minimizes the functional

$$U = \|\partial \mathbf{m}\|^2 + \mu^{-1}\left[\|\mathbf{W}(\mathbf{d} - F(\mathbf{m}))\|^2 - \chi^2\right] \tag{3}$$

where $\mathbf{d}$ is the magnetotelluric data, $F(\mathbf{m})$ is the forward MT response (Key & Ovall, 2011), $\mathbf{W}$ is a diagonal matrix of inverse data standard errors, μ is a regularization factor, χ^2 is a user-defined misfit tolerance, and $\delta\mathbf{m}$ is a model roughness term. The inversion progresses by first automatically sweeping through values of μ to find the best-fitting model and iterating until the χ^2 target misfit is achieved. The second phase of the inversion involves searching for the smoothest model that also achieves the desired misfit. Model updates are performed at each iteration via linearizing the functional about a starting model. The inclusion of the χ^2 tolerance in the functional allows the inversion to avoid extreme local minima based on select noisy or nonphysical data. Data fit is assessed using a root-mean-square (RMS) misfit that is normalized by data errors and the number of variables

$$\mathrm{RMS} = \sqrt{\frac{1}{n}\sum_{i=1}^{n}\left[\frac{d_i - F_i(m)}{s_i}\right]^2} \tag{4}$$

where d_i and $F_i(m)$ are an individual datum and corresponding forward response, s_i is data uncertainty, and n is the total number of data points.

Anisotropy for the purposes of this study refers to strictly horizontal (or transverse) anisotropy, wherein the electrical resistivity of each grid cell is allowed to vary in two directions: parallel (ρ_{yy}) and perpendicular (ρ_{xx}) to the profile trace. It is expected that transverse anisotropic structure oriented at an oblique angle to the profile trace will partition into ρ_{xx} and ρ_{yy} components. Anisotropy is incorporated into the inversion through the model roughness term, which contains a measure of the difference between the ρ_{xx} and ρ_{yy} resistivity models, regularized by an anisotropy penalty factor, α. The value of α varies from 0 (completely anisotropic) to 1 (isotropic) and is defined by the user prior to inversion. For the anisotropic inverse models shown in this study we set $\alpha = 0.1$ to allow the structure to vary in both anisotropic directions.

2.4. Data Preparation

Inputs into the inversion include apparent resistivity and phase of the principal impedances (Z_{XY} and Z_{YX}) and the complex 2-D component of the tipper (T_Y). The apparent resistivity of the transverse electric (TE) mode, $\rho_{a,xy}$, was omitted from the inversion input due to its sensitivity to off-profile (i.e., 3-D) electrical resistivity structure (Wannamaker et al., 1984). The remaining data were decimated to five periods per decade, yielding a total of 30 inverted periods distributed logarithmically over six decades (0.01–10,923 s). A subset of the decimated data (~13%) was manually culled via visual inspection of transfer function curves to eliminate obvious outliers. In total, 2,496 data points distributed across all 23 stations were inverted for 2-D isotropic and anisotropic resistivity structure. Prior to inversion, data errors for apparent resistivity and phase were increased to a minimum threshold, or error floor, of 10% $|Z_{ij}|$, corresponding to an error in phase of 2.8°, to reduce the likelihood of overfitting data points with exceptionally small statistically determined errors. An error floor of 0.03 was applied to all tipper components. Data inputs for the isotropic and anisotropic inversions were identical.

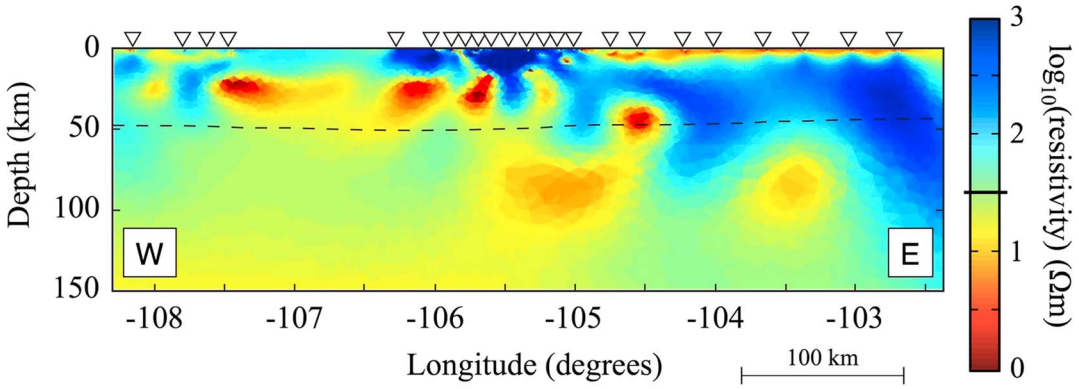

Figure 3. 2-D isotropic electrical resistivity model. The black dashed line is a Moho estimate from Shen et al. (2013). Note the alternating pattern of vertical resistors and conductors suggestive of anisotropic resistivity structure in the lower crust (Figure S2 in the supporting information). The inverted white triangles indicate MT station locations. The bold line on the resistivity color bar indicates starting model resistivity of 30 Ωm.

2.5. Mesh Preparation

Resistivity models for each inversion were parameterized as unstructured meshes using the graphical user interface Mamba2D (http://mare2dem.ucsd.edu/). Mamba2D is a MATLAB-based program that uses Delaunay triangulation to automatically populate regions within the mesh with triangular grid cells of uniform size, where size is defined by the nominal side length of each triangular grid cell. An "area of interest" extending from the surface to 150 km depth (approximately one third of the survey aperture) and 25 km laterally beyond the first and last stations along the profile was divided into three layers. The three horizontal layers are parameterized as follows: 2 km triangles for 0–10 km depth, 5 km triangles for 10–60 km depth, and 10 km triangles for 60–150 km depth. Outside the region of interest, triangles are allowed to grow exponentially in size toward the edges of the model domain that extends 1,000 km in all directions. The atmosphere is parameterized as a 1,000 km thick layer with a fixed resistivity value of 1×10^9 Ωm. Topography is not incorporated into the model. The resistivity of the isotropic half-space starting model, 30 Ωm, was selected by determining which among a series of isotropic half-space models with varying resistivity values exhibited the smallest initial misfit to the data. Model grid parameterization and the starting model for each of the isotropic and anisotropic inversions were identical.

3. Results

3.1. Inversion Results

Figure 3 shows the isotropic resistivity model obtained by inverting the magnetotelluric data along our profile. This model achieved an RMS misfit of 1.3 given the applied errors, representing an 88% reduction in data residual relative to the starting model (initial RMS of 11.3). The alternating pattern of vertical conductive and resistive anomalies visible in the midcrust to upper mantle (25–100 km depth) is reminiscent of the modeling results of Heise and Pous (2001) on the isotropic inversion of anisotropic data. They observed that 2-D isotropic inversions of azimuthally anisotropic magnetotelluric data produce characteristic artifacts in modeled resistivity structure, including alternating regions of high and low resistivities. Motivated by these previous findings and the clear pattern seen in Figure 3, we performed a similar modeling study using MARE2DEM. The results of that study, which can be found in the supporting information, support the hypothesis that some of the structure observed in the isotropic model in Figure 3 is an artifact introduced by insufficient modeling of anisotropic data (Figure S2). For the purposes of model analysis and interpretation going forward we will focus on the anisotropic inversion results.

Figure 4 shows our preferred 2-D horizontally anisotropic resistivity model. The models in Figures 4a and 4b show the electrical resistivity structure perpendicular (ρ_{xx}) and parallel (ρ_{yy}) to profile, respectively. The ρ_{xx} model reflects the resistance to north-south current flow in the direction parallel to inferred geoelectric strike. After seven iterations, our preferred model achieved an RMS of 1.2 given the applied errors, representing an 89% variance reduction relative to the starting model (initial RMS of 11.3). The forward response of the final

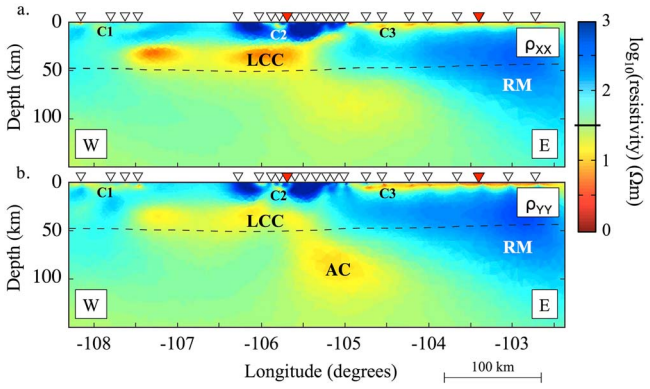

Figure 4. 2-D anisotropic electrical resistivity models. Models for resistivity in (a) N-S (ρ_{xx}) and (b) E-W (ρ_{yy}) directions. Annotations as in Figure 3 plus red triangles denote along-profile location of stations shown in Figure 2. LCC = lower crustal conductor, RM = resistive mantle, AC, C1, C2, C3 = low resistivity anomalies (see text).

model and data fits for two representative stations are shown in Figure 2. Pseudo-sections of the observed data and model response for all stations can be found in Figure S5 in the supporting information.

3.2. Upper Crust

The shallow crust (0–10 km depth) along the profile is resistive with the exception of three thin conductors at or near the surface. These conductors range in resistivity from 5 to 30 Ωm and correlate with the known sedimentary basins labeled in Figure 1. These basins and the corresponding labels in Figure 4 are, from east to west, the westward thickening Denver Basin (C3), the South Park Basin (C2), and the Piceance Basin (C1). The upper crust (0–25 km) outside these conductors is generally resistive (>100 Ωm), reaching a maximum value of 1,000 Ωm beneath the Rocky Mountain Front Range (105°W–106.5°W).

3.3. Lower Crust

The crust beneath the Rocky Mountains is electrically conductive (low resistivity) from midcrustal depths of 25–35 km to the base of the crust at 45–50 km depth (Moho estimates provided by Gilbert, 2012; Sheehan et al., 1995; and Shen et al., 2013). Dense station coverage on the west and east ends of this lower crustal conductor (LCC) constrains its width to ~200 km, from western Colorado to just east of the South Park Basin. Model sensitivity testing (Figure S4 in the supporting information) confirms that the data support a laterally continuous LCC despite the ~100 km gap in station coverage (Figure 1). Magnetotellurics is primarily sensitive to the conductance (conductivity-thickness product) of conductors, and thus, there is a trade-off between the resolvable thickness and absolute conductivity of the LCC (see Figure S3 in the supporting information). Figure 5 shows the vertically integrated conductance along the profile of both the ρ_{xx} and ρ_{yy} models, divided into three layers of equal thickness: upper crust (0–25 km), lower crust (25–50 km), and upper mantle (50–75 km). The conductance of the lower crust beneath the Rocky Mountains is 1,500–2,000 S. In comparison to other regions of our model, the LCC exhibits twice the conductance of the upper mantle directly beneath it, four times that of the Denver Basin (~500 S), and an order of magnitude greater than that of the adjacent lower crust beneath the Great Plains. A lower crustal conductance of 2,000 S is extremely high for tectonically stable lower crust (averaging 40–400 S) (Jones, 1992) but is modest compared to more tectonically active regions such as the Tibetan Plateau (minimum 6,000 S) (Li et al., 2003) and the East African rift (~10 kS) (Desissa et al., 2013). Given the well-resolved top of the LCC and assuming a uniform electrical resistivity for the entire lower crust yield a maximum average resistivity of 12–17 Ωm. Any vertically varying distribution of lower crustal conductivity would thus require the existence of zones of much lower resistivity. Indeed, if the observed lower crustal conductance was confined to a layer 200 m thick within an otherwise resistive crust, the resistivity of that conductor would be only ~0.1 Ωm. Additional petrologic, geologic, and geophysical data are required to reasonably constrain the total thickness and conductivity of this anomaly.

The lower crustal conductor exhibits the strongest degree of anisotropy (anisotropy factor of 2–3) of any feature in the top 75 km of the model (note the separation of conductance curves in Figure 5b). Electrical resistivity in the lower crust appears to be enhanced in the *x* direction (north-south, strike parallel) relative to the *y* direction (east-west, strike perpendicular) (see Figures 4 and 5). Thus, the electrical conductivity in the lower crust is enhanced in a direction parallel or subparallel to both the Rocky Mountain Front and the Rio Grande rift (Figure 1).

The anisotropic behavior we observe could be an artifact of the inversion produced by a series of north-south oriented elongate conductors with finite along strike length (i.e., quasi 3-D conductive bodies parallel to strike). In this scenario, the segmented LCC shown in the isotropic model would be closer to the real Earth structure. We advocate instead for a bulk anisotropy as observed in Figure 4 based on the behavior of the tipper functions over the top of the conductor. The wavelength of the segmented conductors in Figure 3 is on the order of ~20 km. With nominal station spacing over the LCC of 5–10 km we should be able to resolve variability in the tipper due to the presence of strong lateral resistivity contrasts in the lower crust. Pseudo-sections of Parkinson-convention tipper, especially the along profile component (T_{zy}) (Figure S5 in the

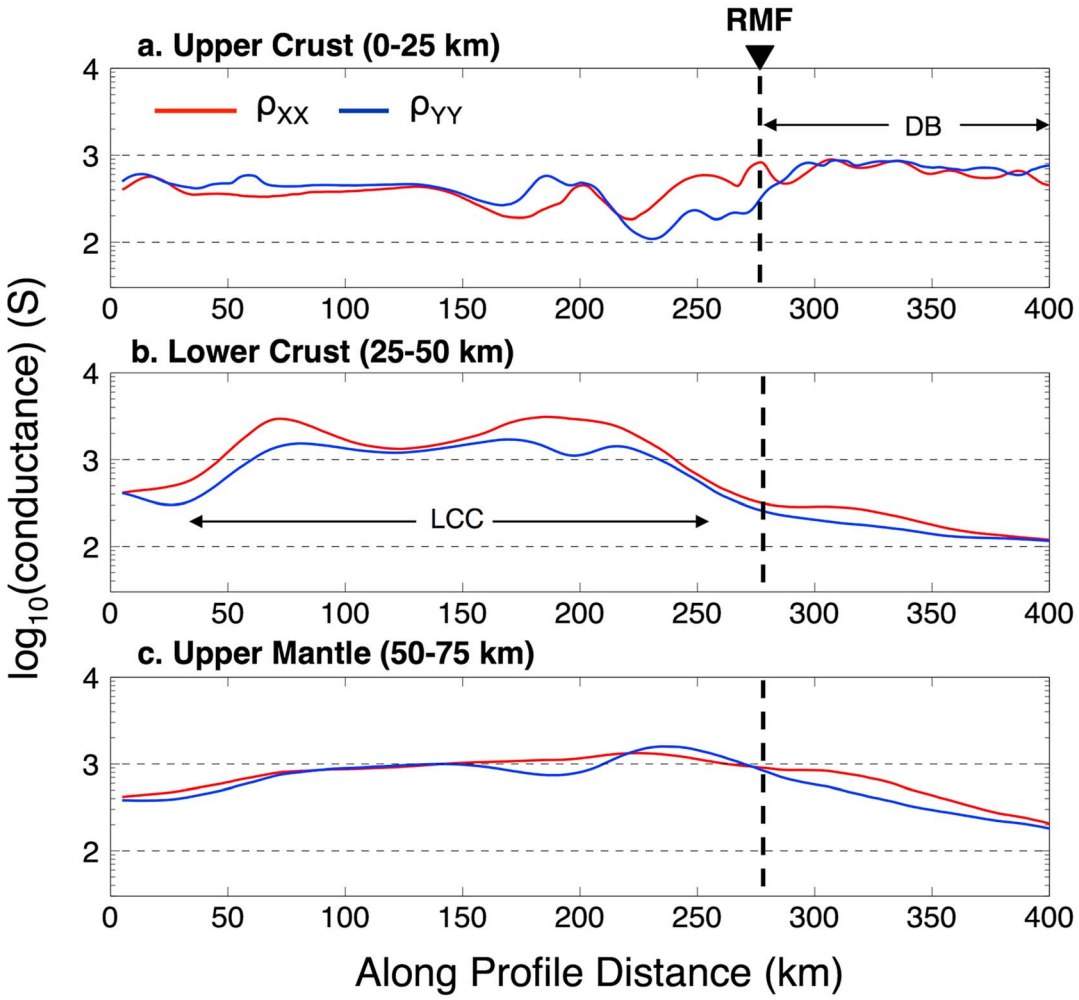

Figure 5. Vertically integrated conductance (conductivity-thickness product) of final ρ_{xx} and ρ_{yy} resistivity models in Figure 4 for (a) upper crust (0–25 km depth), (b) lower crust (25–50 km depth), and (c) upper mantle (50–75 km depth). The bold dashed line indicates location of Rocky Mountain Front (RMF). Conductance along profile shown as separate lines for ρ_{xx} and ρ_{yy} resistivity models, with separation between lines indicating degree of anisotropy. Along profile distance = 0 corresponds to location of westernmost station at approximately (39.2°N, 108.2°W). DB = Denver Basin, LCC = lower crustal conductor.

supporting information), show a binary distribution of induction vector orientations, with western stations pointing east and eastern stations pointing west, toward the interior of the LCC as expected for a laterally cohesive conductor.

3.4. Upper Mantle

The upper mantle in our anisotropic model is electrically conductive ($<$30 Ωm) beneath the Rocky Mountains and increasingly resistive east of the Rocky Mountain Front. An eastward thickening wedge of resistive material extending from the base of the crust into the upper mantle (RM in Figure 4) characterizes the lateral transition from conductive to resistive mantle structure. This is in contrast to a similar lateral transition in the lower crustal resistivity structure that is characterized by a sharp vertical contact located directly beneath the RMF. The gradual increase in upper mantle resistivity to the east is also evident in Figure 5c, which shows gradually decreasing upper mantle conductance east of the RMF. The maximum resistivity observed in the upper mantle lies near the base of the crust on the eastern edge of our profile.

The lowest resistivity in the upper mantle is observed in the ρ_{yy} model directly beneath the Rocky Mountain Front (AC in Figure 4). While this anomaly appears in the model as an isolated body of low resistivity beneath

the Front Range, it is possible that enhanced conductivity in the upper mantle extends to the west, beneath the lower crustal conductor, and/or vertically down into the mantle directly beneath AC. The masking effects of the LCC and limited data coverage west of 106.25°W make the lateral extent of this conductive anomaly difficult to resolve. Similarly, the high conductance of the feature limits our ability to resolve the depth to which it extends into the upper mantle. By ~150 km depth, the upper mantle is conductive ($<$30 Ωm) across the entire profile.

To first order, electrical resistivity structure below 150 km is characterized by subtle variations in resistivity, with a range of resistivity values spanning only half a decade in log-resistivity space (10–30 Ωm) over the entire model from 150 to 300 km depth. Lateral variations are practically nonexistent, and the overall trend is of decreasing resistivity with depth. If our data were sensitive to this type of resistivity structure, we would expect apparent resistivity of the off-diagonal impedance elements to decrease at long periods and for the corresponding phase at those periods to be increasing toward 90°. We do not observe these trends at most stations (e.g., Figure 2a), and when we do (e.g., Figure 2b), we prefer to attribute these effects to the large resistivity contrast in the uppermost mantle (i.e., 50–150 km depth) rather than a subtle resistivity gradient below 150 km. In an effort to limit our interpretation to the minimum structure required by the data, we therefore omit discussion of a possible vertical conductivity gradient in the mantle below 150 km.

4. Discussion

4.1. General Features

Important elements of the 2-D anisotropic resistivity models shown in Figure 4 include (1) a series of thin, near-surface conductors; (2) a crust that is broadly resistive with the exception of the LCC; (3) the lower crustal conductor; and (4) the gradual transition from conductive to resistive upper mantle under the Great Plains. We will address the first two briefly before commenting on the lower crustal conductor and mantle resistivity structure in greater detail. Figure 6 shows an interpretive view of the anisotropic resistivity model with labels corresponding to major features and subsequent interpretation.

The three near-surface conductors (PB, SP, and DB in Figure 6) correlate with three deep sedimentary basins: the Piceance, South Park, and Denver Basins (Figure 1). The low resistivity observed in each of these basins is likely due to the presence of electrically conductive Mesozoic marine shales. These are the Mancos Shale in the Piceance and South Park Basins and a correlating unit, the Pierre Shale, in the Denver Basin (Izett et al., 1971; Maughan, 1988). While the conductivity-thickness trade-off discussed above prevents us from directly measuring the thickness of these sedimentary basins using our 2-D resistivity model, we can derive an estimate for thickness using observed conductance and in situ measurements of electrical resistivity of the geologic units found in these basins. For example, ground and airborne electromagnetic measurements of the Pierre Shale in the Denver Basin show that it is electrically conductive, typically 3–8 Ωm (e.g., Abraham et al., 2012; Ackermann, 1974). Assuming that this unit is responsible for the majority of the upper crustal conductance observed east of the Rocky Mountain Front (~500 S; see Figure 5), we calculate a thickness for the Pierre Shale of 1,500–4,000 m, which is consistent with previously published estimates for that particular unit in the Denver Basin (e.g., 2,420 m (Porter & Weimer, 1982)).

Excluding the lower crustal conductor and the sedimentary basins discussed above, the top 50 km of our anisotropic resistivity model exhibits conductance values of stable tectonic crust (Jones, 1992). The upper crust to the west, beneath the Rocky Mountain Front Range, appears to exhibit substantially greater resistivity ($>$1,000 Ωm) than that of the Great Plains (100–300 Ωm). This contrast is likely in part due to the screening effect of the conductive Denver Basin masking higher resistivity values in the upper crust beneath the Great Plains. The near-surface conductor associated with the Denver Basin is much thicker than estimated depth to resistive basement (Mooney & Kaban, 2010), indicating vertical smearing of this conductor. There is no such screening effect observed for the Rocky Mountain Front Range, where resistive metamorphic and plutonic rocks outcrop at the surface. Previous geophysical studies suggest that the bulk composition of the shallow crust in the southern Rocky Mountains has been altered by repeated intrusion of high-volume silicic magma bodies in the late Cenozoic (Decker et al., 1988; Li et al., 2002; McCoy et al., 2005). Our results do not contradict this interpretation. However, our results do suggest that there is no significant volume of fluid or partial melt in the upper crust today. A large volume of interconnected melt fraction or aqueous fluid in the upper crust would significantly reduce bulk resistivity, which we do not observe.

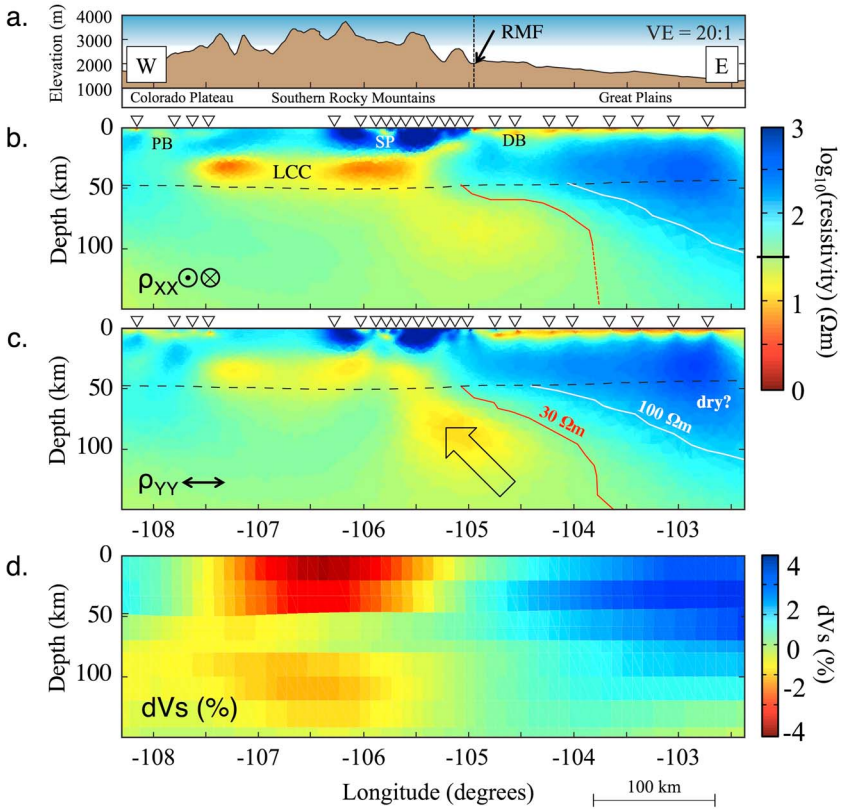

Figure 6. Interpretation of anisotropic electrical resistivity model and comparison to seismic tomography. Resistivity models are identical to Figure 4 for (b) N-S (ρ_{xx}) and (c) E-W (ρ_{yy}) directions. (d) Shear wave velocity perturbation relative to a 1-D-starting model from Li et al. (2002). (a) Topography and approximate physiographic province boundaries along profile. Annotations as in Figure 3 plus white and red lines are approximate resistivity contours for 30 and 100 Ωm, respectively, in the mantle. The arrow in Figure 6c indicates a supply of heat, melt, and/or volatiles to the lithospheric mantle. LCC = lower crustal conductor; DB = Denver Basin; SP = South Park Basin; PB = Piceance Basin; RMF = Rocky Mountain Front.

4.2. Lower Crustal Conductor

The presence of low resistivities in the lower crust and upper mantle is consistent with previous investigations into the electrical resistivity structure of the lithosphere in Colorado. Reitzel et al. (1970) present the results of a large-scale geomagnetic deep-sounding survey of the western United States and find two broad "ridges" of high conductivity in the uppermost mantle, one beneath the southern Rocky Mountains and Rio Grande rift and the other along the Wasatch Front in Utah. Both anomalies are elongate in the north-south direction, parallel to the Rocky Mountain Front. Subsequent modeling of that same data by Porath (1971) yielded two quantitative models of upper mantle resistivity structure that confirmed that high conductivity shallows beneath the Rocky Mountains in Colorado. The techniques used in that study lacked the depth resolution to differentiate between models with high conductivities near the lithosphere-asthenosphere boundary at 150 km, and an alternate but equally well-fitting model with high conductivity near the base of the crust at 45 km. Our results suggest that the model with a shallower conductor in the lower crust and uppermost mantle is the more likely scenario.

The mechanisms most often invoked for explaining low resistivities in the lower crust are highly conductive phases that form interconnected conduction pathways along grain boundaries, including sulfide minerals, graphite films, and fluids such as partial melt or saline brines (Yang, 2011). Kariya and Shankland (1983) show that the resistivity of crustal rocks may also decrease with increasing temperature; e.g., dry basaltic rocks decrease in resistivity from 10^4 to 20 Ωm from 500 to 1,000°C. Low seismic velocities in the upper mantle (e.g., Shen & Ritzwoller, 2016) and elevated crustal geotherms (Decker et al., 1988) suggest that upper mantle and lower crustal temperatures in some regions of the southern Rocky Mountains in Colorado may easily

exceed 1,000°C. Could elevated crustal temperatures, essentially hot dry rock, produce the observed conductivity anomaly in the midcrust to lower crust without the need for additional conductivity mechanisms?

4.2.1. Solid-State Conductivity Mechanisms in the Lower Crust

Kariya and Shankland (1983) compile results from a multitude of laboratory studies to examine the effect of temperature on the bulk resistivity of dry, sub solidus crustal rocks of both mafic and felsic composition. They show that dry rocks of felsic and intermediate compositions do not achieve resistivity values below ~2,000 Ωm, even at elevated temperatures approaching the solidus (~1,000°C). Basaltic rocks can achieve the resistivity required to explain the lower crustal conductor ($\rho < 20$ Ωm), but only at or near the solidus. Adjusting for the effect of pressure on the basalt dry solidus would theoretically allow the lower crust to achieve higher temperatures (and thus lower resistivity) without melting (e.g., maximum temperature of 1,200°C at 50 km depth). However, in order for elevated bulk temperature to account for the observed lower crustal anomaly, the entire crust from 25 km depth to the crust-mantle interface would need to be composed of basalt at or above 1,000°C. Not only are midcrustal temperatures >1,000°C not supported by regional estimates of crustal geotherms (e.g., Decker et al., 1988), several seismic tomography studies argue in favor of a predominantly felsic composition of the lower crust west of the Rocky Mountain Front (e.g., Li et al., 2002; Schmandt et al., 2015). We conclude that if the lower crust is dry, variations in bulk temperature and composition are insufficient to produce the observed conductivity anomaly without additional contributions from grain-boundary conduction mechanisms.

Sulfide mineralization and thin graphite films can be exceptionally conductive and produce significant low-resistivity anomalies in otherwise cold and dry lower crust (e.g., Bedrosian, 2016; Bedrosian & Box, 2016; Boerner et al., 1996). Thin graphite films form when thick packages of carbon-bearing sedimentary rocks, typically deposited in deep marine basins, are subjected to intense heat and pressure, leading to the formation of graphite films along metamorphic fabrics. Sulfide mineralization occurs by a similar process, involving large volumes of sulfide-bearing sedimentary rocks, also typically sourced from deep marine depositional environments. The presence of graphite or sulfide mineralization in the deep crust requires both a geologic source of the appropriate minerals and a tectonic history that includes forces capable of emplacing those minerals in the deep crust. No evidence suggests that central Colorado meets either of these requirements.

The most significant source of sulfide mineralization in Colorado is the "Colorado Mineral Belt" (CMB) (Tweto & Sims, 1963), a collection of sulfide-bearing hydrothermal, volcanic, and plutonic ore-bodies that form a northeast-trending line from the southwest corner of the state to near Boulder, Colorado. The CMB crosses our profile near 106°W longitude, well within the surface projection of the lower crustal conductor. However, the CMB is a relatively narrow feature (~50 km wide at most) and the presence of sulfides near the surface does not require the existence of large volumes of sulfide mineralization at depth. In terms of graphite mineralization, no geologic evidence suggests that a large source volume of carbon-bearing rocks exists in central Colorado.

4.2.2. Partial Melt

We consider saline fluids and partial melt the most likely sources of high conductivity in the lower crust of the southern Rocky Mountains. The inherent nonuniqueness of the magnetotelluric problem and the tendency for conductive bodies to smear vertically in regularized inversion (e.g., Figure S3) make it difficult to differentiate between fluids and melt with MT alone. We will use petrologic, geochemical, and additional geophysical evidence to investigate the likelihood that the imaged conductor is partial melt, saline fluid, or a combination of the two. Figure 7 provides a diagram of the various melt and fluid distributions that we consider below.

We first consider the end-member case in which the high conductivity of the lower crustal conductor is attributed solely to partial melt (Figures 7a and 7b). Annen et al. (2006) describe in detail the type of deep-crustal magma reservoir or "lower crustal hot zone" that could produce the observed conductivity anomaly: Over a protracted period of time, basaltic magma is intermittently or continuously injected into the crust from the underlying mantle as horizontal sills. The basaltic melt then stalls in the midcrust to lower crust either because it is of sufficient density to be neutrally buoyant or because it is sufficiently viscous due to a higher volatile content. The melt then cools and fractionates into more buoyant, andesitic melt that rises toward the surface, leaving behind a basalt residual. Small pipes of basaltic melt may also escape toward the surface (Jacob et al., 2015).

Ample evidence supports the existence of this petrologic model at work in the southern Rocky Mountains in the very recent past. As stated previously, seismic tomography reveals the upper mantle directly beneath the

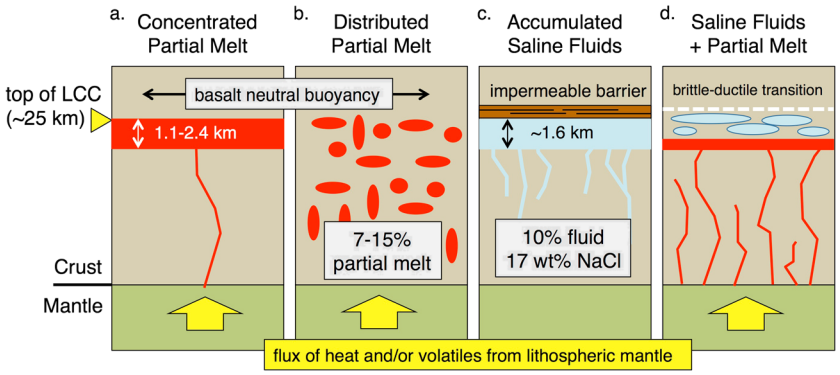

Figure 7. Collection of partial melt and/or fluid distributions that could produce the high conductivity observed in the lower crust beneath the Rocky Mountains, including (a) a series of molten sills, (b) distributed partial melt, (c) saline fluid ponding beneath an impermeable barrier to upward fluid flow, and (d) intermediate combinations of ponded fluid and distributed and/or ponded partial melt. The yellow arrow represents supply of heat and/or volatiles driving production of melt in lithospheric mantle. Preferred interpretation most closely resembles Figure 7d (see text for details).

Rocky Mountains to be anomalously warm (Hansen et al., 2015) and may contain melt that could be supplied to the lower crust (e.g., Humphreys et al., 2003). The presence of melt in the crust would increase seismic attenuation, and Phillips et al. (2014) observe that seismic attenuation of Lg surface waves at frequencies corresponding to crustal depths (0.75–1.5 Hz) is high for most of Colorado west of the Rocky Mountain Front. Levandowski et al. (2014) found that mapping seismic shear wave velocity to density structure overestimates the buoyancy of the crust in central Colorado. They conclude that the presence of crustal melt could produce the observed effect, as partial melt would greatly reduce shear wave speed without significantly altering bulk density. Geotherm estimates from Decker et al. (1988) suggest that the crust beneath the Rio Grande rift in central Colorado (106.25°W along our profile) resides above the basalt dry solidus at depths >36 km and above the alkali basalt saturated solidus at even shallower depths. Lastly, and perhaps most directly relevant, there is a collection of Quaternary age basalt flows in central Colorado, the youngest of which was erupted ~4,150 years before present (Rowe et al., 2015) near Dotsero, CO (Figure 1, blue star). Geochemical analysis performed by Leat et al. (1989) suggests that the Dotsero magmas did experience at least a limited amount of fractional crystallization at pressures appropriate for the lower crust, suggesting that these magmas are associated with a crustal magma reservoir.

Assuming that the elevated electrical conductivity observed in the midcrust to lower crust is the result of a distinct crustal zone containing some unknown melt fraction, we can constrain the physical and petrologic properties of that melt using the work of Waff (1974). The bulk conductivity of a rock hosting partial melt is largely dependent on the electrical conductivity of the melt, the degree to which the melt is connected, and the fraction of the rock that contains partial melt. The contribution of the solid matrix resistivity to the bulk electrical properties of the rock is in most cases negligible. We will need to independently constrain most of these parameters if we are to extract a meaningful interpretation of the imaged MT anomaly.

We start by constraining the various parameters that control the conductivity of the melt. We utilize the online tool SIGMELTS (Pommier & Le-Trong, 2011) that uses a large database of experimental results and empirically derived relationships to constrain the electrical conductivity of a melt based on a variety of physical and chemical parameters. More specifically, SIGMELTS provides a means for calculating silicate melt conductivity as a function of melt temperature, pressure, and composition (wt % H_2O, Na_2O, and SiO_2). Partial melt is only electrically conductive so long as it is fluid, so presumably any melt observable by MT has a minimum temperature above the solidus. The basalt dry solidus for depths of 25–50 km is 1,160°–1,200°C. The solidus for wet basalt in the midcrust is much lower, ~800°C (Decker et al., 1988), due to the effect of water lowering the melting point. In the high-temperature extreme we assume that the melt has recently been extracted from the upper mantle. Hansen et al. (2015) map surface-wave shear velocities to lithospheric temperature for most of the U.S. and find a maximum temperature of ~1,300°C beneath central Colorado at a depth of 82 km. Leat et al. (1989) performed major element geochemistry for 14 rock samples collected from four Quaternary basalt flows in central Colorado, including the Dotsero flow. They found basalts high in sodium (wt % Na_2O = 3.74 ± 0.34%) with silica values typical for basalt (wt % SiO_2 = 49.51 ± 0.84%).

Estimates of wt % H_2O for in situ partial melt are difficult to obtain but can be estimated via analysis of the volatiles present in fluid inclusions. For example, a recent study of late Cenozoic basalts erupted in northern New Mexico estimated the water content of the melt at 0.5–2.0 wt % H_2O (Rowe et al., 2015). To our knowledge, no estimates of in situ water content exist for Quaternary magmas in Colorado, so we will consider the end-member cases of both dry and wet (2 wt % H_2O) basalt. Depth to the top of the conductor (25 km) provides an estimate of the minimum pressure experienced by the melt (~1 GPa). Passing these constraints through the SIGMELTS program yields melt conductivities of 0.6–1.5 S/m for dry basalt and 0.3–3.5 S/m for wet basalt, with the range of melt conductivity values encompassing the range of permissible temperature. Assuming a melt temperature of 1,200°C yields melt conductivities of 0.83 S/m and 1.78 S/m for dry and wet basalt, respectively.

Figure S6 shows the relationship between bulk resistivity of a rock and melt fraction contained within that rock for a melt of a particular conductivity, in this case 0.83 S/m (dry basalt) and 1.78 S/m (wet basalt). The geometrical model that forms the basis for this relationship (Waff, 1974, equation (26)) assumes a small melt fraction ($<$15%), a solid rock matrix that is substantially more resistive than the melt, and a 100% interconnected melt. Owing to the latter assumption, melt fraction estimates from this analysis are minimum values, as a less interconnected melt would require higher melt concentrations to produce the same bulk resistivity values. Because the physical constraints of the magnetotelluric method prohibit the independent determination of the thickness or absolute conductivity of the conductor (see the supporting information), our interpretation is subject to a trade-off between bulk resistivity and melt fraction. In the extreme case that the melt is confined to a single tabular layer of molten rock, or a series of such layers containing nearly 100% melt (Figure 7a), the cumulative thickness of those melt layers would be 1.1 and 2.4 km for the wet and dry basalts, respectively. In the other extreme, where melt is distributed uniformly from 25 km depth to the base of the crust (Figure 7b), the melt fraction in the lower crust would be 7–15% for wet and dry basalts, respectively. We consider this a substantial melt fraction for a relatively amagmatic region of the continental interior. For comparison, Desissa et al. (2013) use magnetotelluric data and a similar analysis to estimate a melt fraction $>$13% for the crust beneath an incipient mid-ocean ridge in the Afar region of the East African rift.

Basaltic underplating and/or injection of molten basalt into the midcrust are expected to result in at least a limited degree of crustal melting. Relatively low seismic velocities in the deep crust (e.g., Li et al., 2002) and a high-magnitude density contrast across the crust-mantle boundary found by Schmandt et al. (2015) suggest that the deep crust beneath Colorado is of intermediate or felsic composition. If we alter the melt parameters in SIGMELTS to simulate the chemical composition of a typical rhyolite (~70% SiO_2 and ~5% Na_2O), we find melt conductivities at 1,200°C of 0.09–0.44 S/m for dry and wet melts, respectively. Assuming a more felsic melt in our interpretation would require a thicker melt layer and/or a higher melt fraction within the melt zone. In interpreting the presence of melt in the lower crust we recognize that a spectrum of melt compositions is likely present, including a felsic component contributed by anatectic melts, especially given the inferred composition of the lower crust in Colorado. However, for the purposes of putting meaningful constraints on melt fraction and melt layer thickness, we restrict our interpretation to high conductivity melts (i.e., basaltic melts) as that assumption provides minimum values of layer thickness and melt fraction well suited for hypothesis testing in subsequent work.

4.2.3. Aqueous Fluid

Another likely source of high conductivity in the lower crust, especially in active tectonic environments, is aqueous fluid (e.g., Li et al., 2003; Wannamaker et al., 2008). Saline fluids in the deep crust can easily exceed the conductivity of seawater ($>$3 S/m) and can produce high conductivity anomalies with far smaller fluid volumes than required for anomalies of similar conductance composed of partial melt. Where it is available, seismic reflection data can be helpful in differentiating aqueous fluid from partial melt in deep-crustal conductors. The concentration of fluids into lenses produces high-impedance contrast "bright spots" in seismic reflection sections that are often coincident with lower crustal conductors (Hyndman & Shearer, 1989). The Continental Dynamics of the Rocky Mountains (CD-ROM) experiment included the acquisition of seismic refraction and reflection data along the crest of the southern Rocky Mountains. At the latitude of our MT profile in central Colorado, Rumpfhuber and Keller (2009) observe a midcrustal reflector in the CD-ROM data at depths similar to the well-resolved top of the lower crustal conductor (22–23 km). However, they suggest that the reflector is a product of the interwedging of crustal blocks from adjacent Proterozoic terranes,

juxtaposed during the assembly of the North American continent, and do not consider the role of fluids in their interpretation.

Absent independent geologic and geophysical evidence for the presence of saline fluid in the deep crust we rely on the results of laboratory studies and estimates of fluid porosity to assess the likelihood that fluids contribute to the observed high conductivity. We do not consider the scenario in which aqueous fluids permeate the entire lower crust. Yardley and Valley (1997) argue that in stable tectonic regimes high-grade metamorphic and igneous rocks of the lower crust will readily incorporate free fluids to produce hydrated retrograde metamorphic minerals and that the lower crust in general behaves as a fluid sink rather than a fluid source. Even in more active tectonic regimes it is difficult to maintain vertically distributed free fluids in the lower crust. The permeability required to produce observable volumes of interconnected free fluid in the lower crust would also facilitate the evacuation of that buoyant fluid to shallower depths.

Figure 7c shows a typical model of fluid distribution that is often invoked to explain low resistivity anomalies in the midcrust to lower crust. In this model, saline fluids are typically interpreted as thin horizons of accumulated fluid ponding beneath impermeable barriers to upward fluid flow (e.g., Eaton, 1980; Hyndman & Shearer, 1989; Jiracek et al., 1983). Eaton (1980) suggests that ductile shear concentrated near the brittle-ductile transition during lithospheric extension may produce a pervasive physical barrier to fluid migration. Fluid flow at midcrustal levels may also be impeded by fluid-rock interactions that reduce permeability, such as silicate precipitation and/or volume increasing hydration reactions (Hyndman & Shearer, 1989). In the former scenario, the LCC indicates depth to the brittle-ductile transition and/or a pervasive midcrustal décollement associated with regional-scale crustal extension. In the latter, the top of the LCC corresponds to the isotherm associated with silicate precipitation and retrograde metamorphism reactions (350–400°C). These interpretations are not mutually exclusive.

Shimojuku et al. (2014) provide estimates of the bulk electrical conductivity of brine-bearing quartzite under midcrustal conditions (T = 800–1,100 K, P = 1 GPa). The most conductive sample tested (quartzite with 30% fluid fraction consisting of 17 wt % NaCl brine) exhibited a bulk conductivity of ~4 S/m, with little variation due to temperature. A layer of brine-bearing quartzite with this porosity and salinity would need to be just 500 m thick in order to produce the observed lower crustal conductance of 2,000 S. Extrapolating to a more modest fluid fraction of 10%, based on examination of midcrustal "bright spots" in Tibet (Caldwell et al., 2009), yields a bulk conductivity of 1.25 S/m, which would require a layer of fluid-bearing rock 1.6 km thick to produce the observed conductance. We consider this the minimum thickness of a brine-bearing rock layer required to produce the observed high conductivity, as thinner layers would require salinity and/or fluid fractions that may not be reasonable for the depths at which high conductivity is observed. Lower salinity and/or porosity would require a thicker layer of fluid accumulation and/or an increasingly high aggregate volume of midcrustal fluid.

4.2.4. Preferred Geologic Model for the Lower Crust

Figure 7d shows our preferred interpretation of the lower crustal conductor, in which both partial melt and saline fluids are present. The end-member cases presented in the previous sections and illustrated in Figures 7a–7c are problematic in that they would not produce the observed strike-parallel anisotropy. We appeal instead to a model in which melt is supplied to the crust via melt-filled fractures, or vertical dikes, aligned parallel to strike. These melt-filled cracks would produce the observed anisotropy by providing a north-south aligned fabric that would preferentially channel electric currents into a strike-parallel direction. These fractures are either sufficiently thin or too closely spaced so as to prevent our model from resolving individual cracks. The north-south orientation of fractures is consistent with the inferred local stress regime. Geodetic observations suggest that much of Colorado is experiencing distributed east-west extension (Berglund et al., 2012), implying that the least principal stress direction is also oriented east-west. Injection of magma into this type of stress regime would produce north-south oriented dikes trending perpendicular to the least principal stress direction.

We cannot rule out the possibility that these strike-parallel fractures are alternatively or simultaneously occupied by transient pulses of aqueous fluid. However, we find it difficult to advocate for a model that does not include some fraction of partial melt. The fluid concentrations required to produce the observed anomaly (up to 10%, see above) would reduce the solidus to the point of melting the crust given the high temperatures modeled for the lower crust in the region (Decker et al., 1988). Furthermore, the independent geophysical

evidence for lower crustal melt and Quaternary volcanism in Colorado described above suggest that a "water-only" model is unlikely.

Our preferred model also includes melt and aqueous fluid ponding at midcrustal levels. These features are added to explain the presence of the lower crustal conductor in the strike perpendicular resistivity model (Figure 4b). These ponded fluids provide a component of isotropic high conductivity at the top of the LCC resolvable in both components of the anisotropic inversion results. Ponded melt is a straightforward consequence of supplying melt to the lower crust, while ponded fluids are expected to result from crust-melt interactions. Possible sources of fluid in this scenario include magmatic fluid exsolving from the partial melt as it cools and metamorphic fluids released by heating of hydrous minerals in the surrounding crust.

4.3. Upper Mantle Resistivity Structure

Seismic tomography, teleseismic traveltime residuals, and receiver function studies suggest a substantial increase in thickness of the subcontinental lithospheric mantle (SCLM) from west to east across the Rocky Mountain Front (e.g., Hansen et al., 2015; Lee & Grand, 1996; Sheehan et al., 1995; Yuan et al., 2014). Sheehan et al. (1995), for example, advocate for a mantle density structure in which the high-density lithospheric mantle lid is 60 km thicker under the Great Plains than it is under the adjacent Southern Rocky Mountains. Our preferred anisotropic electrical resistivity model shows a moderately resistive ($>$50 Ωm) eastward thickening feature in the Great Plains upper mantle extending from the base of the crust to depths of 125–150 km beneath the eastern edge of our profile (RM in Figure 4). Does this transition from conductive to resistive upper mantle represent the electrical lithosphere-asthenosphere boundary (LAB) shallowing to the west? Or is it simply an alteration and/or thermal boundary internal to the mantle lithosphere?

4.3.1. Electrical Lithosphere-Asthenosphere Boundary

We first consider the scenario in which the lateral resistivity structure imaged beneath the Great Plains within the top 150 km of our model reflects the electrical LAB shallowing toward the range front from the east. Dai and Karato (2009) cite typical resistivity values of 10–25 Ωm to calculate moderate bulk water content (100–400 ppm) for typical asthenosphere at 1,300°C. Figure 6 shows an approximate 30 Ωm resistivity contour in the upper mantle of our model east of the range front. If we assume that this contour represents the LAB, we would expect asthenospheric temperatures of $>$1,200°C, and consequently low seismic velocities, to be imaged east of the Rocky Mountain Front at depths $<$100 km.

Seismic tomography studies that utilize surface waves and/or ambient noise are in particular sensitive to seismic velocity structure over the depth range of the most pronounced features in our electrical resistivity models (near surface to 150 km). A number of such studies have been performed across the RMF (Hansen et al., 2015; Li et al., 2002; Shen & Ritzwoller, 2016; Shen et al., 2013). Li et al. (2002), for example, provide a high lateral resolution image of upper mantle velocity perturbations along our profile that shows a sharp lateral contrast in upper mantle velocity structure across a vertical boundary located at ~105°W that persists to depths $>$150 km (Figure 6d). This suggests that the mantle directly east of the range front is cold and likely not asthenosphere. However, more recent seismic tomography studies utilizing the USArray (Shen & Ritzwoller, 2016) and more focused studies using local seismic networks (Hansen et al., 2013) produce conflicting results for model regions within 50–100 km of the Rocky Mountain Front (Figure S7). It is difficult to reconcile our magnetotelluric results with the differing seismic models. We note that all of these seismic studies lack the dense station distribution of the magnetotelluric study, in particular east of the range front, and those that exhibit the easternmost extent of low velocity out into the plains (e.g., Shen & Ritzwoller, 2016) also have the least dense station spacing (~70 km). The thick sedimentary package of the Denver Basin provides an additional complication in the modeling of seismic wave speeds adjacent to the range front and may account in part for the variability observed in the seismic results.

In the scenario in which we assume that we are successfully imaging the electrical LAB east of the range front, the 30 Ωm contour is the minimum depth to that boundary. In reality, the depth to the LAB is likely much deeper than the 30 Ωm contour, especially near the range front where the contour impinges on the base of the crust. We expect that a buffer of lithospheric material of likely indeterminable thickness is present at the base of the crust across our entire profile. Under this assumption, we still must account for the relatively high conductivity (30–100 Ωm) present east of the RMF above the 30 Ωm contour and below the resistive crust, a region of what is most likely subcontinental lithospheric mantle.

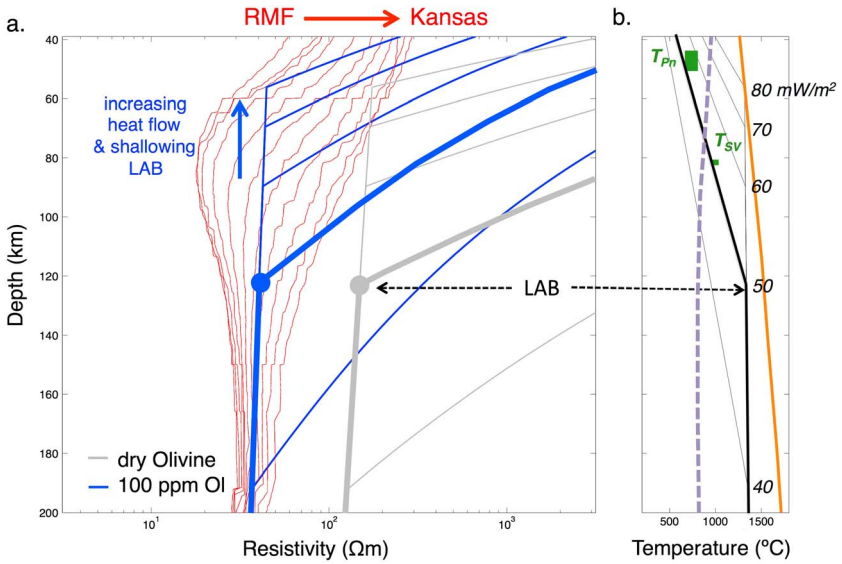

Figure 8. (a and b) Mantle resistivity versus lithospheric hydration. The red lines in Figure 8a are resistivity-depth profiles extracted from Great Plains region of ρ_{xx} model in Figure 4a. The red arrow indicates increasing upper mantle resistivity with eastward progression of profiles from the Rocky Mountain Front (RMF) to near the Colorado-Kansas border. The blue and gray lines are electrical resistivity models (Gardes et al., 2014) for dry (gray) and hydrated (100 ppm H_2O) mantle olivine subject to a range of assumed continental geotherms in Figure 8b (Hasterok & Chapman, 2011). Multiple lines in Figure 8a show the effect of geothermal gradient on resistivity profiles. Geotherms are defined by surface heat flow values (indicated in Figure 8b in units of mW/m^2 at depth that mantle lithosphere geotherm intersects mantle adiabat). The bold lines in Figure 8a represent resistivity models corresponding to preferred geotherm bolded in Figure 8b (50 mW/m^2). Preferred geotherm justified by surface heat flow and seismically derived estimates of mantle temperature (green squares) from Hansen et al. (2015) (T_{SV}) and Schutt et al. (2013) (T_{Pn}). The dashed horizontal line is estimated depth of lithosphere-asthenosphere boundary (LAB) determined from change in slope of geotherm (i.e., depth of transition from conductive to convective geotherm). The orange line is peridotite dry solidus (Hirschmann, 2000), and the purple line is peridotite saturated solidus (Till et al., 2010)

4.3.2. Modification of Subcontinental Lithospheric Mantle

To further examine the distribution of lithospheric mantle material beneath the Great Plains, and to better characterize the physical and chemical state of said lithosphere, we examine typical resistivity values of continental lithospheric mantle under various conditions. Electrical conductivity of the lithospheric mantle may be enhanced by the presence of partial melt, water in nominally anhydrous minerals, and to a lesser extent, elevated bulk temperature. Using the unified olivine conductivity model of Gardes et al. (2014), we estimate that even at exceptionally high temperatures (>1,300°C), the resistivity of the mantle lithosphere cannot achieve resistivity values below ~100 Ωm without the addition of melt and/or hydration. We note that the conductivity model of Gardes et al. is limited to olivine conductivity; however, we do not expect more complex mantle lithologies (e.g., including pyroxenes and garnet) to exhibit substantially higher conductivity under dry conditions. We have plotted an approximate 100 Ωm contour for the upper mantle east of the RMF in Figure 6. In our interpretation, this contour represents the maximum depth to which the lithospheric mantle beneath the plains may be dry and/or melt-free. The resistivity values observed below the 100 Ωm contour are incompatible with unmodified SCLM. Although the 100 Ωm contour represents a minimum threshold for dry conditions, we expect that modification also extends above this line given that seismic estimates of upper mantle temperature at these depths (~1,000°C; Hansen et al., 2015) are still too low to account for observed resistivity $<10^3$ Ωm (Constable et al., 1992).

Estimates of dissolved water content of the lithospheric mantle beneath the Great Plains are constrained by the analysis represented in Figure 8. This figure was inspired by a similar analysis performed by Bedrosian (2016) to assess hydration of the SCLM beneath the Midwestern United States. Figure 8a shows several resistivity versus depth profiles for the Great Plains upper mantle taken from the 2-D resistivity model in Figure 4a. Vertical resistivity profiles are extracted from a region of the model extending laterally from just east of the RMF to the eastern edge of the model near the Colorado-Kansas border. The resistivity model was sampled at an interval of ~20 km. For comparison, the model profiles have been plotted together with resistivity-depth

profiles calculated using a model for olivine resistivity as a function of dissolved water content and temperature (Gardes et al., 2014). We assume a conductive mantle geotherm for the region, accounting for variable heat production and a surface heat flow of 40–80 mW/m^2 (Hasterok & Chapman, 2011), with the different resistivity models in Figure 8a representing results obtained assuming the various geotherms shown in Figure 8b. Note that the geotherms converge to a mantle adiabat with potential temperature of 1,400°C. Models for anhydrous and hydrous (100 ppm H_2O) olivine are shown. Also plotted in Figure 8b are the dry peridotite solidus (orange line; Hirschmann, 2000), the saturated peridotite solidus (purple line; Till et al., 2010), and two seismically derived estimates of upper mantle temperature in eastern Colorado from Hansen et al. (2015) and Schutt et al. (2013).

We can draw several conclusions about the physical state of the lithosphere east of the Rocky Mountain Front from examination of Figure 8. The primary observation is that the modeled electrical resistivity is predominantly inconsistent with a dry lithospheric mantle. The "water-free" olivine resistivity model (Figure 8a, gray lines) only approaches the model resistivity profiles for the easternmost profiles assuming the highest geothermal gradients. Surface heat flow actually decreases with distance east of the range front, and near the Colorado-Kansas border is well below the 70–80 mW/m^2 values that would be indicative of the thermal regime required to produce the observed resistivity in the mantle lithosphere. If we assume that partial melting of dry lithosphere was contributing to the low resistivity, we would expect the geothermal gradient to exceed the peridotite dry solidus over a significant depth range coincident with the observed low resistivity. This is not the case for even the warmest lithospheric temperature profile (Figure 8b). Thus, our preferred electrical resistivity model is incompatible with a "water-free" mantle lithosphere beneath the Great Plains, at least to the eastern extent of our profile.

We observe two clear patterns in the resistivity profiles from our anisotropic model: (1) the average bulk resistivity of the upper mantle increases from west to east and (2) the depth to the minimum resistivity increases along the same trend; i.e., the profiles become steeper toward Kansas. If we interpret the first trend in terms of water content, the implication is that dissolved water concentration in the mantle increases toward the range front, with maximum hydration occurring beneath the RMF. The second trend, a steepening of the resistivity profile, is consistent with the behavior observed for a decrease in geothermal gradient, or thickening of the lithosphere. That we observe steepening of the profiles from west to east suggests that the lithosphere may be thickening to the east. We emphasize, however, that the resistivity values throughout the model are too low for variations in lithospheric thickness to fully account for conductivity increasing toward the range front.

We consider the qualitative observation of a hydrated lithosphere east of the Rocky Mountain Front to be our most important finding with regard to upper mantle resistivity structure. The observation of a gradual change in resistivity structure beneath the plains is equally significant in that it suggests that RMF transition zone is not as abrupt in the mantle lithosphere as it may be in the crust. The following attempts to further quantify the amount of water dissolved in the upper mantle are presented to confirm that hydration is a reasonable interpretation and aid in future hypothesis testing.

We observe from Figure 8a that the resistivity profiles derived from the MT results fit an olivine resistivity model with water content of 100 ppm much better than that of anhydrous olivine. While hydrous olivine may be responsible for the majority of high conductivity in the upper mantle, estimates of bulk mantle water content and subsequent assessment of whether those estimates are reasonable must take into consideration other nominally anhydrous minerals.

We can use the method of Sarafian et al. (2015) to convert mantle olivine water content into bulk mantle water content based on modal proportions of peridotite minerals and partition coefficients. Assuming 100 ppm water in olivine and a pyrolite composition of olivine:orthopyroxene:garnet = 60:25:15 yields a bulk mantle water content $>$400 ppm or $>$0.04 wt % H_2O. This value is relatively high but not unreasonable compared to other magnetotelluric determinations of lithospheric water content (e.g., 10^{-2} wt %; Selway et al., 2014).

Partial melt may also contribute to the high conductivity beneath the westernmost Great Plains. No direct evidence from seismic tomography (e.g., Li et al., 2002) (Figure 6d), body wave attenuation (Boyd & Sheehan, 2005), seismicity (Nakai et al., 2017), surface geology, or heat flow suggests that there are any active or recently active magmatic systems beneath the Great Plains in eastern Colorado at this latitude. However, plotting the saturated peridotite solidus (Till et al., 2010), along with reasonable estimates of continental

geotherms for this region (Figure 8b), shows that conditions in the upper mantle may permit partial melting of hydrous peridotite. We speculate that partial melt beneath the western plains could represent a possible reservoir or melt pathway for the partial melt present in the lower crustal conductor. Indeed, the anisotropic (east-west conductive) anomaly AC in Figure 4b may reflect the lateral transport of the proposed melt.

4.3.3. Upper Mantle Structure West of the RMF

We limit our discussion of the upper mantle resistivity structure west of the Rocky Mountain Front to a few broad observations, given that screening effects of the lower crustal conductor severely limit our ability to resolve mantle structure and the resistivity contrasts in the mantle below it are expected to be slight. The upper mantle beneath the southern Rocky Mountains appears to be generally conductive (~30 Ωm) and isotropic (Figure 5c). Seismic tomography and receiver function studies indicate that the lithosphere-asthenosphere boundary is relatively shallow beneath the southern Rocky Mountains, perhaps at depths $<$90 km (e.g., Sheehan et al., 1995). The resistivity values observed beneath the LCC at those depths are consistent with modeled asthenospheric resistivity (30 Ωm for 100 ppm H_2O asthenosphere; Dai & Karato, 2009). However, lithospheric mantle that has been hydrated and/or infiltrated by partial melt, as suggested, for example, by Humphreys et al. (2003), is expected to exhibit similarly low resistivity values. This lithospheric stratigraphy is in contrast to that of the more energetic Snake River Plain magmatic region near Yellowstone, which exhibits resistivity values in the upper mantle consistent with dry lithosphere (Meqbel et al., 2014). The low resistivity lithosphere beneath the southern Rocky Mountains suggests that melt and/or fluids persist in the upper mantle and remain to be fluxed through this less active magmatic system.

Thinned lithosphere beneath the SRM is a plausible explanation for the observed resistivity structure, although it is unlikely that we can independently constrain lithospheric thickness in this portion of the model. Petrologic and geophysical evidence suggests that lithospheric stratigraphy beneath the southern Rocky Mountains in Colorado consists of heavily modified lower crust (this study), hot and/or partially molten mantle lithosphere (e.g., Humphreys et al., 2003), and hydrous asthenosphere, none of which is expected to be resistive. Determining lithospheric thickness in this type of tectonic environment (i.e., imaging the boundary between two conductive layers of the upper mantle) would be difficult even without the masking effects of the LCC. In terms of upper mantle structure beneath the LCC, we appeal to the existing interpretations from the seismic community (i.e., thinned lithosphere) and note that our data do nothing to refute that hypothesis.

4.4. Tectonic Implications

4.4.1. Partial Melt in the Lower Crust

In interpreting the lower crustal conductor we must consider the timing of fluid emplacement, the source of fluids, and the spatial scale of the anomaly. Partial melt emplaced in the midcrust is not at thermal equilibrium with the surrounding rock and will freeze over several thousands to millions of years, depending on the volume and frequency of repeated injection and initial crustal temperature (Annen et al., 2006). Yardley and Valley (2000) argue that saline brines in the lower crust can only persist as free fluids for a limited geologic time before the chemical, thermal, and pressure conditions of the lower crust that favor hydration reactions will consume those fluids in retrograde metamorphism. The width of the lower crustal resistivity anomaly dictates that any mechanism we invoke for supplying fluids to the lower crust must be capable of producing laterally pervasive crustal modification. The high conductivity that we image is therefore the result of recent tectonic activity that has provided volatiles, heat, and/or magma to a broad area of the lower crust in the very recent past and/or in a sustained manner over the last few million years.

It is reasonable to assume that the partial melt that we interpret to exist in the midcrust to lower crust is the result of melting of the lithosphere. Humphreys et al. (2003) argue that low seismic velocity in the upper mantle beneath the southern Rocky Mountains represents hot, dry, and perhaps partially molten lithospheric mantle. Leat et al. (1989) advocate for a lithospheric mantle source for the Quaternary lavas erupted in central Colorado. Lithospheric melting is achieved through three mechanisms: the addition of heat, the addition of volatiles, and/or decompression melting. The first two mechanisms may also supply free fluids to the lower crust, either as exsolved magmatic fluids or fluids released from high-temperature metamorphic reactions of previously hydrated minerals.

Small-scale convection of the upper mantle is one plausible mechanism for melting the mantle lithosphere. The advection of heat, volatiles, and/or partially molten asthenosphere to the base of the lithosphere could all contribute to partial melting of lithospheric mantle. Geodynamic modeling by van Wijk et al. (2010) suggests

that small-scale edge-driven convection can initiate at a step in lithospheric thickness. They suggest that this process is in part responsible for initiation of the Rio Grande rift at the boundary between the Colorado Plateau and Great Plains in New Mexico, where the Great Plains crust and lithosphere are much thicker than that of the Colorado Plateau today (Wilson et al., 2005). Section 4.3 describes the evidence for a differential lithospheric thickness across the Rocky Mountain Front in Colorado that could be responsible for the initiation of edge-driven convection in the sublithospheric mantle.

Determining the mechanism responsible for the initiation and continuation of small-scale convection beneath Colorado, or otherwise supplying melt to the lower crust, is left for future geodynamic modeling studies. We speculate, based on modest estimates of Cenozoic extension at the surface, that there are processes at work other than rifting, unless the mantle lithosphere has become substantially decoupled from the overlying crust. A mechanically destabilized lower crust could provide another means of initiating convection. The presence of water in the lower crust, especially at volumes suggested by the water-rich end-member case discussed above (Figure 7c), could weaken and destabilize the crust (e.g., Jackson et al., 2004). If the lower crust is also antibuoyant, for example, after basaltic underplating has densified the crust-mantle interface, one could imagine a scenario in which foundering of lithosphere into a shallow asthenosphere could generate decompression melting.

Electrical conductivity of the upper mantle is enhanced directly beneath the RMF (AC in Figure 4b and arrow in Figure 6). This anomaly appears to be anisotropic as well, with conductivity enhanced in the east-west direction, perpendicular to geoelectric strike (Figure 6c). We speculate that this resistivity structure reflects a flux of partial melt and fluids into the mantle lithosphere from an east-west directed convection cell upwelling beneath the Rocky Mountain Front transition zone. The 200 km width of the lower crustal conductor may represent some characteristic length scale of this inferred convection cell, wherein melt and fluids flux out of the sublithospheric mantle as material moves from east to west, ultimately downwelling beneath western Colorado.

4.4.2. Hydration of the Lithospheric Mantle

The possible identification of pervasive hydration of the lithospheric mantle east of the Rocky Mountain Front has implications for the tectonic evolution and modification history of the continental interior. An apparent eastward decrease in the degree of modification to the SCLM is consistent with progressive dewatering during subduction of the eastward-dipping Farallon slab. A similar mechanism for supplying water to the mantle has been proposed for more active tectonic regions to the west (e.g., Humphreys et al., 2003) and has been invoked to explain kimberlite eruptions in eastern Kansas in the Late Cretaceous (Currie & Beaumont, 2011). It is difficult to constrain the hydration state east of the range front due to (1) a low availability of extrusive volcanism to provide direct sampling of lithospheric mineralogy and water content and (2) the minor H_2O concentration in nominally anhydrous minerals that has a negligible effect on bulk density and seismic velocity. The penetration of hydrous phases into the uppermost mantle has implications for the ability of water to migrate through the lithosphere and may help explain the presence of hydrated mineral phases in lower crustal rocks above relatively thick lithosphere (Jones et al., 2015). One interpretation of the so-called "ignimbrite flare-up" (Lipman, 1992) is that pervasive mantle hydration and refrigeration provided by the Farallon slab primed the lithospheric mantle for melting upon slab removal and exposure to high temperature asthenosphere. The reason the hydrated western plains did not follow a similar volcanic progression is unclear, although our results show that hydrous partial melt may reside in the Great Plains lithosphere today.

5. Conclusions

We present a 2-D anisotropic electrical resistivity model of the crust and upper mantle beneath the southern Rocky Mountains and Great Plains. We identify two significant features that have implications for the tectonic evolution of the boundary between stable Proterozoic lithosphere of the western Great Plains and recently modified lithosphere of the southern Rocky Mountains: (1) a broad zone (200 km wide) of low resistivity ($<$20 Ωm) located at 25 km depth beneath the highest topography in Colorado and (2) lower than expected resistivity in the upper mantle east of the range front that we interpret as an eastward deepening "hydration front" extending into the lithospheric mantle beneath the Great Plains. Interpreting the lower crustal conductor in the context of petrologic and geophysical constrains, we eliminate temperature, composition, graphite, and sulfide mineralization as the primary source of high conductivity. End-member petrologic models that may explain the high conductivity include ubiquitous basaltic melt in the midcrust to lower

crust (7–15% melt fraction), a several kilometer thick sequence of mafic sills recently injected into the midcrust, and an accumulation of saline fluid ponding at the brittle-ductile transition. The reality is likely some combination of these readily quantifiable end-member scenarios involving both saline fluids and partial melt (Figure 7d), such as north-south oriented magmatic dikes that periodically supply basaltic magma and exsolved magmatic fluids to midcrustal levels. We speculate that basaltic magma in the lower crust beneath the Rocky Mountains is the result of partial melting of the lithospheric mantle driven by the addition of heat and/or volatiles from below. The existence of partial melt in the lower crust indicates that the southern Rocky Mountains remain tectonically active. We speculate that edge-driven convection initiated along a step in lithospheric thickness may play a significant role in driving that tectonic activity. The increase in upper mantle conductivity with depth beneath the Great Plains likely represents a modification gradient internal to the subcontinental lithospheric mantle, although a westward thinning lithosphere may also be observed. Hydration of the SCLM beneath the plains, possibly accomplished by dewatering of the shallowly subducting Farallon slab in the early Cenozoic, has implications for the tectonic evolution of the continental interior worthy of further investigation.

Acknowledgments

The authors thank the Editor and an anonymous reviewer for constructive comments and suggestions. The authors thank Craig Jones, Lang Farmer, Peter Molnar, Jared Peacock, and Ned Sterne for valuable discussions. We thank Kerry Key and the Seafloor Electromagnetic Methods Consortium for the use of MARE2DEM and advice on its use. Our magnetotelluric data were collected over two summer field campaigns through a joint effort by the U.S. Geological Survey and the University of Colorado Boulder. Instrumentation was provided by the U.S. Geological Survey in Denver, CO, and by Martyn Unsworth at the University of Alberta. This work was supported by the University of Colorado Boulder Geological Sciences Department Spetzler and W.O. Thompson awards, the Rocky Mountain Association of Geologists Bolyard Scholarship, the Society of Exploration Geophysicists, the Geological Society of America, and National Science Foundation grants EAR-1249669 and EAR-1053596. Additional support was provided by the National Science Foundation EarthScope grant (EAR-0323309). This work would not have been possible without land access granted by the National Forest Service, the State of Colorado, James Mark Jones State Wildlife Area, Douglas County Colorado, and numerous private landowners. Various maps and graphics were created using Generic Mapping Tools (Wessel & Smith, 1991). Thanks to Aibing Li, Steven Hansen, and Weisen Shen for providing their seismic tomography models. Magnetotelluric transfer function estimates and time series used in this analysis are available through a U. S. Geological Survey data release hosted on ScienceBase (https://doi.org/10.5066/F7610XTR).

References

Abraham, J. D., Cannia, J. C., Bedrosian, P. A., Johnson, M. R., Ball, L. B., & Sibray, S. S. (2012). Airborne electromagnetic mapping of the base of aquifer in areas of western Nebraska. *U.S. Geological Survey Scientific Investigations Report, 2011–5219*.

Ackermann, H. D. (1974). Shallow seismic compressional and shear wave refraction and electrical resistivity investigations at Rocky Flats, Jefferson County, Colorado. *Journal of Research of the U.S. Geological Survey*, *2*(4), 421–430.

Annen, C., Blundy, J. D., & Sparks, R. S. J. (2006). The genesis of intermediate and silicic magmas in deep crustal hot zones. *Journal of Petrology*, *47*(3), 505–539. https://doi.org/10.1093/petrology/egi084

Bedrosian, P. A. (2016). Making it and breaking it in the Midwest: Continental assembly and rifting from modeling of EarthScope magnetotelluric data. *Precambrian Research*, *278*, 337–361. https://doi.org/10.1016/j.precamres.2016.03.009

Bedrosian, P. A., & Box, S. E. (2016). Highly conductive horizons in the Mesoproterozoic Belt-Purcell Basin: Sulfidic early basin strata as key markers of Cordilleran shortening and Eocene extension. In J. S. MacLean & J. W. Sears (Eds.), *Belt basin: window to Mesoproterozoic Earth*. *Geological Society of America Special Paper*, *522*, 305–339. https://doi.org/10.1130/2016.2522(12)

Berglund, H. T., Sheehan, A. F., Murray, M. H., Roy, M., Lowry, A. R., Nerem, R. S., & Blume, F. (2012). Distributed deformation across the Rio Grande Rift, Great Plains, and Colorado Plateau. *Geology*, *40*(1), 23–26. https://doi.org/10.1130/G32418.1

Boerner, D. E., Kurtz, R. D., & Craven, J. A. (1996). Electrical conductivity and Paleo-Proterozoic foredeeps. *Journal of Geophysical Research*, *101*(B6), 13,775–13,791. https://doi.org/10.1029/96JB00171

Booker, J. R. (2014). The magnetotelluric phase tensor: A critical review. *Surveys in Geophysics*, *35*, 7–40. https://doi.org/10.1007/s10712-013-9234-2

Boyd, O. S., & Sheehan, A. F. (2005). Attenuation tomography beneath the Rocky Mountain Front: Implications for the physical state of the upper mantle. In *The Rocky Mountain region: An evolving lithosphere* (pp. 361–377). Washington, DC: American Geophysical Union.

Caldwell, T. G., Bibby, H. M., & Brown, C. (2004). The magnetotelluric phase tensor. *Geophysical Journal International*, *158*, 457–469. https://doi.org/10.1111/j.1365-246X.2004.02281.x

Caldwell, W. B., Klemperer, S. L., Rai, S. S., & Lawrence, J. F. (2009). Partial melt in the upper-middle crust of the northwest Himalaya revealed by Rayleigh wave dispersion. *Tectonophysics*, *477*, 58–65. https://doi.org/10.1016/j.tecto.2009.01.013

Chapin, C. E., & Cather, S. M. (1994). Tectonic setting of the axial basins of the northern and central Rio Grande rift. In G. R. Keller, & S. M. Cather (Eds.), *Basins of the Rio Grande Rift: Structure, stratigraphy, and tectonic setting*. *Geological Society of America Special Paper*, *291*, 5–26. https://doi.org/10.1130/SPE291-p5

Constable, S. C., Parker, R. L., & Constable, C. G. (1987). Occam's inversion: A practical algorithm for generating smooth models from electromagnetic sounding data. *Geophysics*, *52*(3), 289–300.

Constable, S., Shankland, T. J., & Duba, A. (1992). The electrical conductivity of an isotropic olivine mantle. *Journal of Geophysical Research*, *97*(B3), 3397–3404. https://doi.org/10.1029/91JB02453

Currie, C. A., & Beaumont, C. (2011). Are diamond-bearing Cretaceous kimberlites related to low-angle subduction beneath western North America? *Earth and Planetary Science Letters*, *303*, 59–70.

Dai, L., & Karato, S. (2009). Electrical conductivity of orthopyroxene: Implications for the water content of the asthenosphere. *Proceedings of the Japan Academy. Series B, Physical and Biological Sciences*, *85*, 466–475. https://doi.org/10.2183/pjab.85.466

DeCelles, P. G. (2004). Late Jurassic to Eocene evolution of the Cordilleran thrust belt and foreland basin system, western U.S.A. *American Journal of Science*, *304*, 105–168.

Decker, E. R., Heasler, H. P., Buelow, K. L., Baker, K. H., & Hallin, J. S. (1988). Significance of past and recent heat-flow and radioactivity studies in the Southern Rocky Mountains region. *Geological Society of America Bulletin*, *100*, 1851–1885.

Desissa, M., Johnson, N. E., Whaler, K. A., Hautot, S., Fisseha, S., & Dawes, G. J. K. (2013). A mantle magma reservoir beneath an incipient mid-ocean ridge in Afar, Ethiopia. *Nature Geoscience*, *6*, 861–865. https://doi.org/10.1038/ngeo1925

Dickinson, W. R., Klute, M. A., Hayes, M. J., Janecke, S. U., Lundin, E. R., McKittrick, M. A., & Olivares, M. D. (1988). Paleogeographic and paleotectonic setting of Laramide sedimentary basins in the central Rocky Mountain region. *Geological Society of America Bulletin*, *100*, 1023–1039.

Eaton, G. P. (1980). Geophysical and geological characteristics of the crust of the Basin and Range province. In *Studies in geophysics-continental tectonics* (pp. 96–113). Washington, DC: National Academy of Science.

Eaton, G. P. (1987). Topography and origin of the southern Rocky Mountains and Alvarado Ridge. In M. P. Coward, J. F. Dewey, & P. L. Hancock (Eds.), *Continental extensional tectonics*. *Geological Society Special Publication*, *28*, 355–369.

Eaton, G. P. (2008). Epeirogeny in the Southern Rocky Mountains region: Evidence and origin. *Geosphere*, *4*(5), 764–784. https://doi.org/10.1130/GES00149.1

Egbert, G. D. (1997). Robust multiple-station magnetotelluric data processing. *Geophysical Journal International*, *130*, 475–496.

Epis, R. C., & Chapin, C. E. (1975). Geomorphic and tectonic implications of the post-Laramide, late Eocene erosion surface in the Southern Rocky Mountains. *Geological Society of America Memoirs*, *144*, 45–74.

Fenneman, N. M. (1946). Physical divisions of the United States. One map (scale 1:7,500,000). Reston, VA: U.S. Geological Survey.
Gamble, T. D., Goubau, W. M., & Clarke, J. (1979). Magnetotellurics with a remote magnetic reference. *Geophysics*, *44*(1), 53–68.
Gardes, E., Gaillard, F., & Tarits, P. (2014). Toward a unified hydrous olivine electrical conductivity law. *Geochemistry, Geophysics, Geosystems*, *15*, 4984–5000. https://doi.org/10.1002/2014GC005496
Gilbert, H. (2012). Crustal structure and signatures of recent tectonism as influenced by ancient terranes in the western United States. *Geosphere*, *8*(1), 141–157. https://doi.org/10.1130/GES00720.1
Hansen, S. M., Dueker, K., & Schmandt, B. (2015). Thermal classification of lithospheric discontinuities beneath USArray. *Earth and Planetary Science Letters*, *431*, 36–47. https://doi.org/10.1016/j.epsl.2015.09.009
Hansen, S. M., Dueker, K. G., Stachnik, J. C., Aster, R. C., & Karlstrom, K. E. (2013). A rootless rockies—Support and lithospheric structure of the Colorado Rocky Mountains inferred from CREST and TA seismic data. *Geochemistry, Geophysics, Geosystems*, *14*, 2670–2695. https://doi.org/10.1002/ggge.20143
Hasterok, D., & Chapman, D. S. (2011). Heat production and geotherms for the continental lithosphere. *Earth and Planetary Science Letters*, *307*, 59–70. https://doi.org/10.1016/j.epsl.2011.04.034
Heise, W., & Pous, J. (2001). Effects of anisotropy on the two-dimensional inversion procedure. *Geophysical Journal International*, *147*, 610–621.
Hirschmann, M. M. (2000). Mantle solidus: Experimental constraints and the effects of peridotite composition. *Geochemistry, Geophysics, Geosystems*, *1*(10), 1042. https://doi.org/10.1029/2000GC000070
Humphreys, E., Hessler, E., Dueker, K., Farmer, G. L., Erslev, E., & Atwater, T. (2003). How Laramide-age hydration of North American lithosphere by the Farallon slab controlled subsequent activity in the Western United States. *International Geology Review*, *45*(7), 575–595. https://doi.org/10.2747/0020-6814.45.7.575
Hyndman, R. D., & Shearer, P. M. (1989). Water in the lower continental crust: Modelling magnetotelluric and seismic reflection results. *Geophysical Journal International*, *98*, 343–365.
Izett, G. A., Cobban, W. A., & Gill, J. R. (1971). The Pierre Shale near Kremmling, Colorado, and its correlation to the East and the West. *U.S. Geological Survey Professional Paper, 684-A*.
Jackson, J. A., Austrheim, H., McKenzie, D., & Priestley, K. (2004). Metastability, mechanical strength, and the support of mountain belts. *Geology*, *32*, 625–628. https://doi.org/10.1130/G20397.1
Jacob, K. H., Farmer, G. L., Buchwaldt, R., & Bowring, S. A. (2015). Deep crustal anatexis, magma mixing, and the generation of epizonal plutons in the Southern Rocky Mountains, Colorado. *Contributions to Mineralogy and Petrology*, *169*(7), 1–23. https://doi.org/10.1007/s00410-014-1094-3
Jiracek, G. R., Gustafson, E. P., & Mitchell, P. S. (1983). Magnetotelluric results opposing magma origin of crustal conductors in the Rio Grande Rift. *Tectonophysics*, *94*, 299–326.
Jones, A. G. (1992). Electrical conductivity of the continental lower crust. In D. M. Fountain, R. J. Arculus, & R. W. Kay (Eds.), *Continental lower crust* (pp. 81–143). Amsterdam: Elsevier.
Jones, C. H., Mahan, K. H., Butcher, L. A., Levandowski, W. B., & Farmer, G. L. (2015). Continental uplift through crustal hydration. *Geology*, *43*(4), 355–358. https://doi.org/10.1130/G36509.1
Kariya, K. A., & Shankland, T. J. (1983). Electrical conductivity of dry lower crustal rocks. *Geophysics*, *48*(1), 52–61.
Key, K. (2016). MARE2DEM: A 2-D inversion code for controlled-source electromagnetic and magnetotelluric data. *Geophysical Journal International*, *207*, 571–588. https://doi.org/10.1093/gji/ggw290
Key, K., & Ovall, J. (2011). A parallel goal-oriented adaptive finite element method for 2.5-D electromagnetic modelling. *Geophysical Journal International*, *186*, 137–154. https://doi.org/10.1111/j.1365-246X.2011.05025.x
Landman, R. L., & Flowers, R. M. (2013). (U-Th)/He thermochronologic constraints on the evolution of the northern Rio Grande Rift, Gore Range, Colorado, and implications for rift propagation models. *Geosphere*, *9*(1), 170–187. https://doi.org/10.1130/GES00826.1
Leat, P. T., Thompson, R. N., Dickin, A. P., Morrison, M. A., & Hendry, G. L. (1989). Quaternary volcanism in northwestern Colorado: Implications for the roles of asthenosphere and lithosphere in the genesis of continental basalts. *Journal of Volcanology and Geothermal Research*, *37*, 291–310.
Lee, D., & Grand, S. P. (1996). Upper mantle shear structure beneath the Colorado Rocky Mountains. *Journal of Geophysical Research*, *101*(B10), 22,233–22,244. https://doi.org/10.1029/96JB01502
Levandowski, W. B., Jones, C. H., Shen, W., Ritzwoller, M. H., & Schulte-Pelkum, V. (2014). Origins of topography in the western U.S.: Mapping crustal and upper mantle density variations using a uniform seismic velocity model. *Journal of Geophysical Research: Solid Earth*, *119*, 2375–2396. https://doi.org/10.1002/2013JB010607
Li, A., Forsyth, D. W., & Fischer, K. M. (2002). Evidence for shallow isostatic compensation of the southern Rocky Mountains from Rayleigh wave tomography. *Geology*, *30*(8), 683–686.
Li, S., Unsworth, M. J., Booker, J. R., Wei, W., Tan, H., & Jones, A. G. (2003). Partial melt or aqueous fluid in the mid-crust of Southern Tibet? Constraints from INDEPTH magnetotelluric data. *Geophysical Journal International*, *153*, 289–304.
Lipman, P. W. (1992). Magmatism in the Cordilleran United States; Progress and problems. In B. C. Burchfiel, P. W. Lipman, & M. L. Zoback (Eds.), *The geology of North America, The Cordilleran orogen: Conterminous U.S* (pp. 481–514). Boulder, CO: The Geological Society of America.
Mallory, W. W. (1958). Pennsylvanian coarse arkosic redbeds and associated mountains in Colorado. In *Symposium on Pennsylvanian rocks of Colorado and adjacent areas* (pp. 17–20). Denver, CO: Rocky Mountain Association of Geologists.
Maughan, E. K. (1988). Geology and petroleum potential, Colorado Park Basin Province, North-Central Colorado. *U.S. Geological Survey Professional Paper Open File Rep., 88-450 E*.
McCoy, A., Roy, M., Trevino, L., & Keller, G. R. (2005). Gravity modeling of the Colorado Mineral Belt. In K. E. Karlstrom & G. R. Keller (Eds.), *The Rocky Mountain region: An evolving lithosphere tectonics, geochemistry, and geophysics*, *Geophysical Monograph Series* (Vol. 154, pp. 71–90). Washington, DC: American Geophysical Union.
Meqbel, N. M., Egbert, G. D., Wannamaker, P. E., Kelbert, A., & Schultz, A. (2014). Deep electrical resistivity structure of the northwestern U.S. derived from 3-D inversion of USArray magnetotelluric data. *Earth and Planetary Science Letters*, *402*, 290–304.
Mitrovica, J. X., Beaumont, C., & Jarvis, G. T. (1989). Tilting of continental interiors by the dynamical effects of subduction. *Tectonics*, *8*(5), 1079–1094.
Mooney, W. D., & Kaban, M. K. (2010). The North American upper mantle: Density, composition, and evolution. *Journal of Geophysical Research*, *115*, B12424. https://doi.org/10.1029/2010JB000866
Nakai, J. S., Sheehan, A. F., & Bilek, S. L. (2017). Seismicity of the Rocky Mountains and Rio Grande Rift from the EarthScope Transportable Array and CREST temporary seismic networks, 2008-2010. *Journal of Geophysical Research: Solid Earth*, *122*, 2173–2192. https://doi.org/10.1002/2016JB013389

Pakiser, L. C., & Zietz, I. (1965). Transcontinental crustal and upper-mantle structure. *Reviews of Geophysics*, *3*(4), 505–520.
Phillips, W. S., Mayeda, K. M., & Malagnini, L. (2014). How to invert multi-band, regional phase amplitudes for 2-D attenuation and source parameters: Tests using the USArray. *Pure and Applied Geophysics*, *171*, 469–484. https://doi.org/10.1007/s00024-013-0646-1
Poe, B. T., Romano, C., Nestola, F., & Smyth, J. R. (2010). Electrical conductivity anisotropy of dry and hydrous olivine at 8 GPa. *Physics of the Earth and Planetary Interiors*, *181*, 103–111. https://doi.org/10.1016/j.pepi.2010.05.003
Pommier, A., & Le-Trong, E. (2011). "Sigmelts": A web portal for electrical conductivity calculations in geosciences. *Computers and Geosciences*, *37*, 1450–1459. https://doi.org/10.1016/j.cageo.2011.01.002
Porath, H. (1971). Magnetic variation anomalies and seismic low-velocity zone in the Western United States. *Journal of Geophysical Research*, *76*, 2643–2648. https://doi.org/10.1029/JB076i011p02643
Porritt, R. W., Allen, R. M., & Pollitz, F. F. (2014). Seismic imaging east of the Rocky Mountains with USArray. *Earth and Planetary Science Letters*, *402*, 16–25. https://doi.org/10.1016/j.epsl.2013.10.034
Porter, K. W., & Weimer, R. J. (1982). Diagenetic sequence related to structural history and petroleum accumulation: Spindle Field, Colorado. *AAPG Bulletin*, *66*(12), 2543–2560.
Reitzel, J. S., Gough, D. I., Porath, H., & Anderson, C. W. III (1970). Geomagnetic deep sounding and upper mantle structure in the Western United States. *Geophysical Journal of the Royal Astronomical Society*, *19*, 213–235.
Rowe, M. C., Lassiter, J. C., & Goff, K. (2015). Basalt volatile fluctuations during continental rifting: An example from the Rio Grande Rift, USA. *Geochemistry, Geophysics, Geosystems*, *16*, 1254–1273. https://doi.org/10.1002/2014GC005649
Rumpfhuber, E., & Keller, G. R. (2009). An integrated analysis of controlled and passive source seismic data across an Archean-Proterozoic suture zone in the Rocky Mountains. *Journal of Geophysical Research*, *114*, B08305. https://doi.org/10.1029/2008JB005886
Sarafian, E., Evans, R. L., Collins, J. A., Elsenbeck, J., Gaetani, G. A., Gaherty, J. B., … Lizarralde, D. (2015). The electrical structure of the central Pacific upper mantle constrained by the NoMelt experiment. *Geochemistry, Geophysics, Geosystems*, *16*, 1115–1132. https://doi.org/10.1002/2014GC005709
Schmandt, B., & Humphreys, E. (2010). Complex subduction and small-scale convection revealed by body-wave tomography of the western United States upper mantle. *Earth and Planetary Science Letters*, *297*, 435–445. https://doi.org/10.1016/j.epsl.2010.06.047
Schmandt, B., & Lin, F.-C. (2014). *P* and *S* wave tomography of the mantle beneath the United States. *Geophysical Research Letters*, *41*, 6342–6349. https://doi.org/10.1002/2014GL061231
Schmandt, B., Lin, F.-C., & Karlstrom, K. E. (2015). Distinct crustal isostasy trends east and west of the Rocky Mountain Front. *Geophysical Research Letters*, *42*, 10,290–10,298. https://doi.org/10.1002/2015GL066593
Schutt, D., Lowry, A. R., Buehler, J. S., & Blackwell, D. D. (2013). *The temperature of the western United States lithosphere and areas of likely mantle compositional variations*. Abstract MR43A-2382 Presented at the 2013 AGU Fall Meeting, San Francisco, CA.
Selway, K., Yi, J., & Karato, S.-I. (2014). Water content of the Tanzanian lithosphere from magnetotelluric data: Implications for cratonic growth and stability. *Earth and Planetary Science Letters*, *388*, 175–186.
Sheehan, A. F., Abers, G. A., Jones, C. H., & Lerner-Lam, A. L. (1995). Crustal thickness variations across the Colorado Rocky Mountains from teleseismic receiver functions. *Journal of Geophysical Research*, *100*(B10), 20,391–20,404. https://doi.org/10.1029/95JB01966
Shen, W., & Ritzwoller, M. H. (2016). Crustal and uppermost mantle structure beneath the United States. *Journal of Geophysical Research: Solid Earth*, *121*, 4306–4342. https://doi.org/10.1002/2016JB012887
Shen, W., Ritzwoller, M. H., & Schulte-Pelkum, V. (2013). A 3-D model of the crust and uppermost mantle beneath the Central and Western US by joint inversion of receiver functions and surface wave dispersion. *Journal of Geophysical Research: Solid Earth*, *118*, 1–15. https://doi.org/10.1029/2012JB009602
Shimojuku, A., Yoshino, T., & Yamazaki, D. (2014). Electrical conductivity of brine-bearing quartzite at 1 GPa: Implications for fluid content and salinity of the crust. *Earth, Planets and Space*, *66*(2), 1–9. https://doi.org/10.1186/1880-5981-66-2
Till, C. B., Elkins-Tanton, L. T., & Fischer, K. M. (2010). A mechanism for low-extent melts at the lithosphere-asthenosphere boundary. *Geochemistry, Geophysics, Geosystems*, *11*, Q10015. https://doi.org/10.1029/2010GC003234
Tweto, O. (1979). The Rio Grande Rift system in Colorado. In *Rio Grande Rift: Tectonics and magmatism* (pp. 33–56). Washington, DC: American Geophysical Union. https://doi.org/10.1029/SP014p0033
Tweto, O., & Sims, P. K. (1963). Precambrian ancestry of the Colorado Mineral Belt. *Geological Society of America Bulletin*, *74*, 991–1014.
van Wijk, J. W., Baldridge, W. S., van Hunen, J., Goes, S., Aster, R., Coblentz, D. D., … Ni, J. (2010). Small-scale convection at the edge of the Colorado Plateau: Implications for topography, magmatism, and evolution of Proterozoic lithosphere. *Geology*, *38*(7), 611–614. https://doi.org/10.1130/G31031.1
Waff, H. S. (1974). Theoretical considerations of electrical conductivity in a partially molten mantle and implications for geothermometry. *Journal of Geophysical Research*, *79*(26), 4003–4010. https://doi.org/10.1029/JB079i026p04003
Walker, J. D., Bowers, T. D., Black, R. A., Glazner, A. F., Farmer, G. L., & Carlson, R. W. (2006). A geochemical database for western North American volcanic and intrusive rocks (NAVDAT). In A. K. Sinha (Ed.), *Geoinformatics: Data to knowledge*, *Geological Society of America Special Paper* (Vol. 397, pp. 61–71). https://doi.org/10.1130/2006.2397(05)
Wannamaker, P. E., Hasterok, D. P., Johnston, J. M., Stodt, J. A., Hall, D. B., Sodergren, T. L., … Unsworth, M. J. (2008). Lithospheric dismemberment and magmatic processes of the Great Basin-Colorado Plateau transition, Utah, implied from magnetotellurics. *Geochemistry, Geophysics, Geosystems*, *9*, Q05019. https://doi.org/10.1029/2007GC001886
Wannamaker, P. E., Hohmann, G. W., & Ward, S. H. (1984). Magnetotelluric responses of three-dimensional bodies in layered earths. *Geophysics*, *49*(9), 1517–1533.
Wessel, P., & Smith, W. H. F. (1991). Free software helps map and display data. *Eos, Transactions American Geophysical Union*, *72*, 441–446.
Wilson, D., Aster, R. C., Ni, J., Grand, S. P., West, M., Gao, W., … Semken, S. (2005). Imaging the seismic structure of the crust and upper mantle beneath the Great Plains, Rio Grande Rift, and Colorado Plateau using receiver functions. *Journal of Geophysical Research*, *110*, B05306. https://doi.org/10.1029/2004JB003492
Yang, X. (2011). Origin of high electrical conductivity in the lower continental crust: A review. *Surveys in Geophysics*, *32*, 875–903. https://doi.org/10.1007/s10712-011-9145-z
Yardley, B. W. D., & Valley, J. W. (1997). The petrologic case for a dry lower crust high that rise to a fluid pressure to the rock that is still hot and ductile, the fluid pressure. *Journal of Geophysical Research*, *102*(B6), 12,173–12,185. https://doi.org/10.1029/97JB00508
Yardley, B. W. D., & Valley, J. W. (2000). Reply [to "Comment on 'The petrologic case for a dry lower crust' by Bruce W. D. Yardley and John W. Valley"]. *Journal of Geophysical Research*, *105*(B3), 6065–6068. https://doi.org/10.1029/1999JB900323
Yuan, H., French, S., Cupillard, P., & Romanowicz, B. (2014). Lithospheric expression of geological units in central and eastern North America from full waveform tomography. *Earth and Planetary Science Letters*, *402*, 176–186. https://doi.org/10.1016/j.epsl.2013.11.057